Description of photo-association in an ultra-cold gas

van Heel, A.P.G.

Award date:
1995

Description of photo-association in an ultra-cold gas

October 1994

A. van Heel

Report on a graduation project at the Theoretical Physics group at the TUE, Eindhoven.
Supervisors: Prof. Dr. B.J. Verhaar and Ir. H.M.J.M. Boesten.

Contents

Summary

A hot topic in recent cold-atom physics is furnished by collisions between ultra-cold atoms ($T \leq 1$ mK). This ultra-cold temperature regime is particularly interesting because of the possibilities for very high resolution spectroscopy, as has recently been shown by several experimental groups. Comparison of the experimental spectroscopic data, such as the so-called photo-association spectra, and theoretical model calculations can be used to improve the (badly known) interaction potential between two colliding ground-state atoms. These potentials are crucial for experiments in the ultra-cold temperature regime. For instance atomic collisions put severe limits on the present attempts to improve the Cs atomic clock by means of an atomic fountain. Furthermore they determine whether the condensate in future Bose-Einstein condensation experiments will be stable.

This graduation report deals with the theoretical description of photo-association of ultra-cold alkali atoms. In that connection the following subjects have been studied:

The potentials of the excited states of identical alkali dimers have been calculated and the symmetry properties of these states have been determined.
The (internal) molecular states have been extended in that the molecular rotation has been taken into account, resulting in "generalised" kets that also explicitly specify the total molecular angular momentum (including molecular rotation) and its projection on a space-fixed axis.

In the calculation of photo-association spectra two further ingredients are of fundamental importance: the relative contributions of the relative atomic orbital angular momenta (i.e. the rotational quantum numbers) in the ground-state and the matrix elements associated with the photo-association transitions.
The former have been determined using a a simplified model. The angular dependent part of the transition matrix element has been calculated exactly, using the above-mentioned "generalised" kets. This part entails the important selection rules that govern the photo-association process.

Chapter 1

Introduction

The origin of this work is a direct consequence of the rapid and fascinating developments in recent cold-atom physics. In 1985 it was first demonstrated that it is possible to cool Na-atoms to temperatures of 50-100 mK [1]. Only a few years later it was shown that these cold atoms could be stored in so-called traps [2]. Since then, the possibility to cool and trap neutral atoms near absolute zero has led to many new experiments. These developments for example, resulted in the construction of a high precision Cs atomic clock [3].
Furhtermore, the way is now paved towards new experiments, such as the possible demonstration of Bose-Einstein Condensation (B.E.C.). This collective quantum phenomenon can only be achieved at extremely low temperatures because the thermal atomic De Broglie wavelength λ_D needs to be of the same order of magnitude as the average distance between the atoms. Another prerequisite to achieve B.E.C. is a positive sign of the so-called scattering length that is determined by the particular behaviour of the potential governing the collision between two atoms.
In all experiments in the ultracold temperature regime atomic *collisions* play a crucial role. In the Cs-clock for example, these collisions determine the stability of the clock [4] and, as was already mentioned, the particular collisional behaviour of two atoms determines whether or not B.E.C. can occur. Clearly, for a good description of ultracold collisions detailed knowledge of the scattering-potentials is required. There are a couple of ways to determine these scattering potentials.
The most accurate potentials for alkali-dimers are generally obtained spectroscopically, from which data the bound-state (rovibrational) energy levels in the potential can be determined. An RKR-procedure is then used to derive the classical turning points associated with these levels, yielding a first approximation to the potentials. These potentials can then be improved by the so-called IPA method [5]. This is the procedure followed for the Cs+Cs singlet levels in [6]. The problem with a potential of this kind is that usually only the lower energy part of the potential (i.e. radially its inner part) is determined this way. This is partly due to the fact that the RKR method is less suitable for the highest bound states and for heavier alkali atoms it is due to the highest states being too strongly mixed by the atomic hyperfine coupling which destroys the pure singlet and triplet character. In our group we have been able to use collisional frequency shifts in high-precision

atomic clocks to show that the Cs+Cs triplet and singlet scattering lengths are negative [7]. Also for the light elements Li and Na our group has been succesful in obtaining similar information applying an IPA procedure + a new cumulated radial phase method [8].

Apart from K_2, the Rb_2-ground-state potentials, however, are worst known of all alkali-dimers at this moment. The inaccuracy in these potentials for instance prohibits to make definite predictions about the possibilty to achieve B.E.C. in an ultracold Rb-gas. So in view of present and future experiments it is important to determine accurate Rb_2-potentials.

Fortunately there are two experiments at ultra-cold temperatures that look very promising to extract accurate ground-state potentials for Rb. In the first experiment the atoms are trapped by means of a dc magnetic field. The collisions between the atoms in this Magnetic Trap (MT) result in loss of atoms from the trap. These trap-loss collisions can be used to determine the potential between the colliding atoms. For the other experiment an optical Far-Off-Resonance Trap (FORT) is used. In this experiment, the so-called photo-association spectra associated with the absorption and emission of laser photons during the collision of two atoms, can be used to derive very accurate information about the potentials of the colliding atoms. Both experiments are discussed in chapter 2.

In chapter 3 we will first discuss the "state of the art" Rb_2-potentials. It will be shown that these potentials can effectively be described by several parameters. Given the large inaccuracy in the potentials, however, it is very important to decide which of the above mentioned experiments looks most promising to improve the Rb_2-potential parameters. This appears to be the FORT-experiment, because it is possible in this set-up to exclude singlet scattering so only triplet potential parameters are involved in the analysis of these experimental spectra. Our further discussion will therefore be restricted to the analysis of cold atomic collisions in the FORT.

The rest of this report prepares the ingredients for this analysis. In chapter 4 we shall introduce a set of "generalised" kets for the characterisation of atomic collisions (read: molecular states). These kets not only specify "internal" molecular quantum numbers (like the electronic spin S), but also contain information about molecular rotation. In chapter 5 we discuss the interactions between two ground-state atoms and the interactions between a ground and an excited atom. Upon using the "kets" from chapter 4, we can assign several symmetry labels to the molecular states that emerge in the FORT photo-association experiment and we will calculate the long-range molecular potential curves corresponding to these states.

Using the results of chapters 4 and 5, we are able to calculate the relative transition probabilty ("production rate") of excited molecular states out of Rb_2 continuum ground-states. This calculation is rather subtle because it is not clear beforehand how the wave-function of the initial free Rb_2-state must be "normalised". Furhtermore the relative contributions of the relative atomic orbital angular momenta in the ground-state will be determined. In the second part of chapter 6 the angular dependent part of the matrixelement associated with the above mentioned transition will be calculated exactly. This part entails the important selection rules that govern the photo-association spectra.

A summary of the conclusions of this work is given in chapter 7.

Chapter 2

Magnetic and far-off-resonance trap

In this chapter we will discuss two kinds of traps in which (ultra)cold Rb-atoms can be stored. In the first section we discuss two new cooling mechanisms in magnetic traps (MT). The first mechanism is the so-called gravitational Sisyphus cooling and is studied by Cornell et al. at JILA. The second one is the so-called rf-induced evaporative cooling method which is currently being studied by Ketterle et al. at MIT.
In the second section we discuss is the (optical) Far-Off-Resonance Trap (FORT), studied by Heinzen et al. at the university of Texas. In both sorts of traps collisions occur that can lead to loss of atoms from the trap which can be measured experimentally. These so-called trap-loss collisions look very promising to determine accurate Rb_2 ground-state potentials.

2.1 Magnetic traps

In this section we will discuss two experiments that are currently performed by Cornell et al. at JILA, Boulder and by Ketterle et al. at MIT, Cambridge. These experiments look very promising to extract Rb_2 ground-state potential parameters from the measured loss of atoms from the trap.

In both experiments the atoms are trapped by means of the well-known magnetic dipole-force. In the traps that we shall discuss the atoms are cooled by new and rather subtle cooling techniques. In the experiment by Cornell et al. the atoms are cooled by "gravitational Sisyphus cooling" while in the experiment of Ketterle et al., so-called evaporative cooling, resulting from an rf-field is used to reduce the temperature of the trapped atoms.
Before turning to the description of these cooling techniques, we will first discuss the trapping principle in a dc magnetic trap. We shall therefore consider the internal potential energy of a ground-state atom in a dc magnetic field.

The Hamiltonian that effectively describes a ground-state atom in a magnetic field, is given by

$$H^{int} = \frac{a}{\hbar^2}\vec{s}\cdot\vec{i} + (\gamma_e\vec{s} - \gamma_n\vec{i})\cdot\vec{B}, \tag{2.1}$$

where $\vec{s}$ and $\vec{i}$ denote the electon and nuclear spin respectively, γ_e and γ_n are the electronic and nuclear gyromagnetic factors and $\vec{B}$ is the magnetic field; the constant a determines the hyperfine-splitting of the ground-state levels in zero magnetic field.
The first term is the Fermi-contact term and the second term represents the Zeeman-interaction. The Fermi-contact term is invariant under simultaneous rotations of $\vec{s}$ and $\vec{i}$, while the Zeeman term remains invariant under seperate rotations of $\vec{s}$ and $\vec{i}$ around $\vec{B}$. Therefore the component of the total atomic spin $\vec{f} = \vec{s} + \vec{i}$ in the direction of the magnetic field, m_f, is conserved. The eigenstates of (3.1) can thus be labeled by the quantum number m_f. Note that in the limit $B \rightarrow 0$, the total spin quantum number f also becomes a good (conserved) quantum number. For the sake of convenience, an m_f-eigenstate for which the total spin quantum number in the limit $B \rightarrow 0$ tends to the value f shall therefore be denoted by $|f, m_f>$.

For ^{87}Rb, $i = 3/2$ and $s = 1/2$, so there are three eigenstates ($m_f = -1, ., 1$) that connect to the $f = 1$-level and five states ($m_f = -2, ..., 2$) that connect to the $f = 2$-level. There are two eigenstates corresponding to each of the labels $m_f = -1, ., 1$; one of these eigenstates connects to the $f = 1$-level, the other one connects to the $f = 2$-level. The associated eigenvalues and eigenstates are thus found upon diagonalising 2×2-matrices [13]. The resulting internal potential energies, as a function of the magnetic field, are shown in fig 2.1.

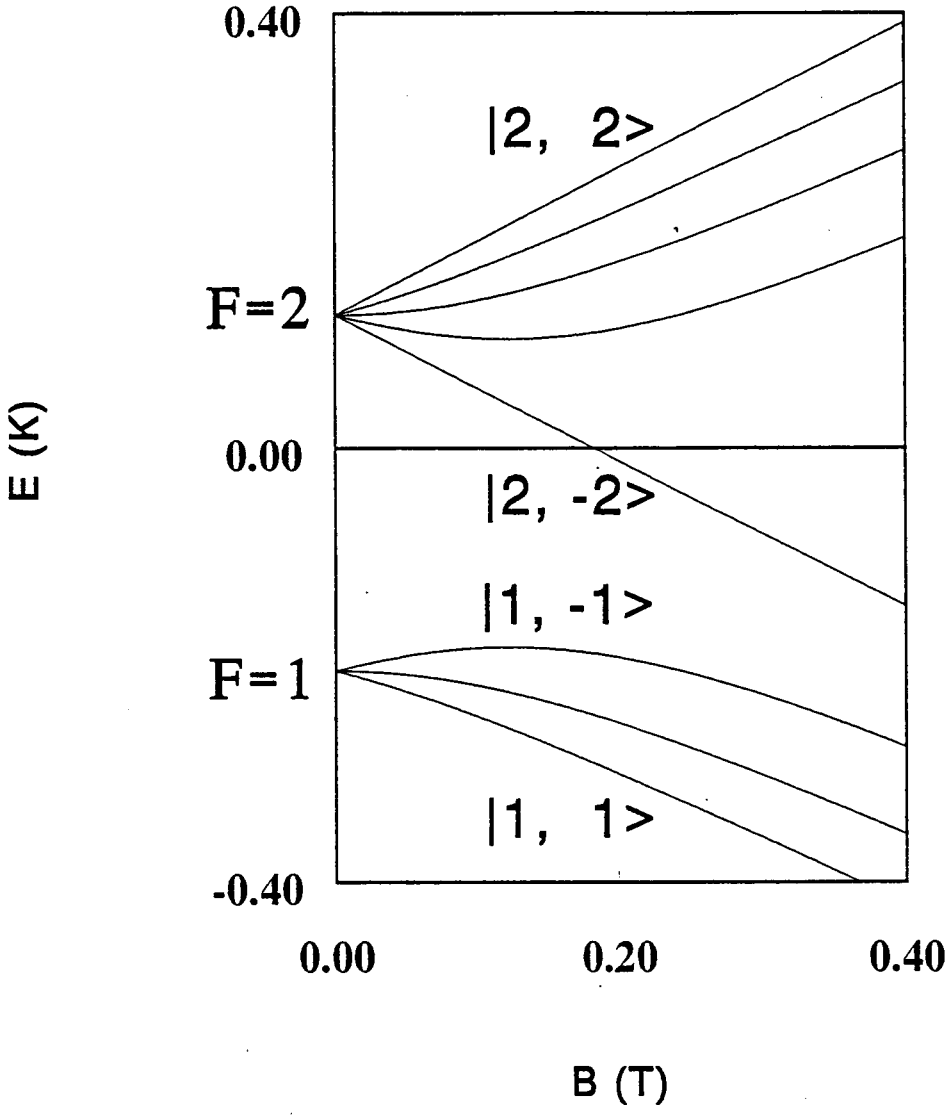

Figure 2.1: Potential energy of the hyperfine states of ^{87}Rb in a magnetic field

In the next two subsections we will show that, for the cooling mechanisms we are interested in, the $f = 1$ states play an important role. Note that of these states only the $m_f = -1$-state, for small values of B, experiences an increasing internal potential energy if the magnetic field increases. A small external magnetic field can therefore be used to provide a confining potential well (=trap) for $|1, -1>$-atoms: the $|1, -1>$-state can thus be *trapped* near the minimum of the magnetic field.
In the next subsections we shall discuss the two earlier-mentioned cooling mechanisms in a dc magnetic trap.

2.1.1 Gravitational Sisyphus cooling

Gravitational Sisyphus cooling is a new and promising method to cool neutral atoms. In the JILA-experiment ^{87}Rb-atoms are optically pumped into the (trappable) $|1,-1>$-state and held in a dc magnetic trap.
This trap is generated by a "baseball" coil that provides a *confining* magnetic field that increases quadratically in all three coordinates x, y and z. In order to keep the atoms near the geometric center of this trap, an extra (vertical) magnetic field gradient, provided by two anti-Helmholz coils, that cancels the gravity on the $|1,-1>$-state, is applied. The atoms in the $|1,-1>$-state are then pumped into the (also trappable) $|2,1>$-state by a two-photon excitation using rf and micro-wave radiation [14].

The internal potential energies of the $|1,-1>$ and the $|2,1>$ states are given by

$$E_{|2,1>} = \frac{-a}{4} - \hbar B\gamma_n + \frac{1}{2}\sqrt{4a^2 + 2a\hbar B(\gamma_e+\gamma_n) + \hbar^2B^2(\gamma_e+\gamma_n)^2}, \tag{2.2}$$

$$E_{|1,-1>} = \frac{-a}{4} + \hbar B\gamma_n - \frac{1}{2}\sqrt{4a^2 - 2a\hbar B(\gamma_e+\gamma_n) + \hbar^2B^2(\gamma_e+\gamma_n)^2}. \tag{2.3}$$

Thus in the limit for small values of B (only keeping terms linear in B), these energies become

$$E_{|2,1>} = \frac{3a}{4} + \frac{1}{4}\hbar B(\gamma_e - 3\gamma_n), \tag{2.4}$$

$$E_{|1,-1>} = \frac{-5a}{4} + \frac{1}{4}\hbar B(\gamma_e + 5\gamma_n). \tag{2.5}$$

Since B varies quadratically in z, the corresponding *internal* energy curves are parabolas. Note, however, that the magnetic moment of the $|2,1>$ state $(= \hbar(\gamma_e - 3\gamma_n)/4)$ is just slightly smaller than the magnetic moment of the $|1,-1>$ state $(= \hbar(\gamma_e + 5\gamma_n)/4)$, so the $|1,-1>$-parabola has a greater curvature than the $|2,1>$-parabola.

In addition to this *internal* energy, the atoms also have *gravitational* potential energy. The total potential energy of the two states in the magnetic field $B = [\beta z^2 - [4mg/\hbar(\gamma_e + 5\gamma_n)]z]$ therefore becomes

$$\begin{aligned} E_{|2,1>} &= \frac{3a}{4} + \frac{1}{4}\hbar(\gamma_e - 3\gamma_n)\left[\beta z^2 - \frac{4mg}{\hbar(\gamma_e+5\gamma_n)}z\right] + mgz \\ &= \frac{3a}{4} + \frac{1}{4}\hbar(\gamma_e - 3\gamma_n)\beta\left[z + \frac{16mg\gamma_n}{\beta\hbar(\gamma_e+5\gamma_n)(\gamma_e-3\gamma_n)}\right]^2 \\ &\quad - \frac{\hbar(\gamma_e-3\gamma_n)\beta}{4}\{\frac{16mg\gamma_n}{\beta\hbar(\gamma_e+5\gamma_n)(\gamma_e-3\gamma_n)}\}^2, \end{aligned} \tag{2.6}$$

$$E_{|1,-1>} = \frac{-5a}{4} + \frac{1}{4}\hbar(\gamma_e + 5\gamma_n)\,\beta z^2. \tag{2.7}$$

In the first line, the term βz^2 represents the quadratic magnetic field generated by the "baseball" coil. The second (linear) term in the square brackets accounts for the extra

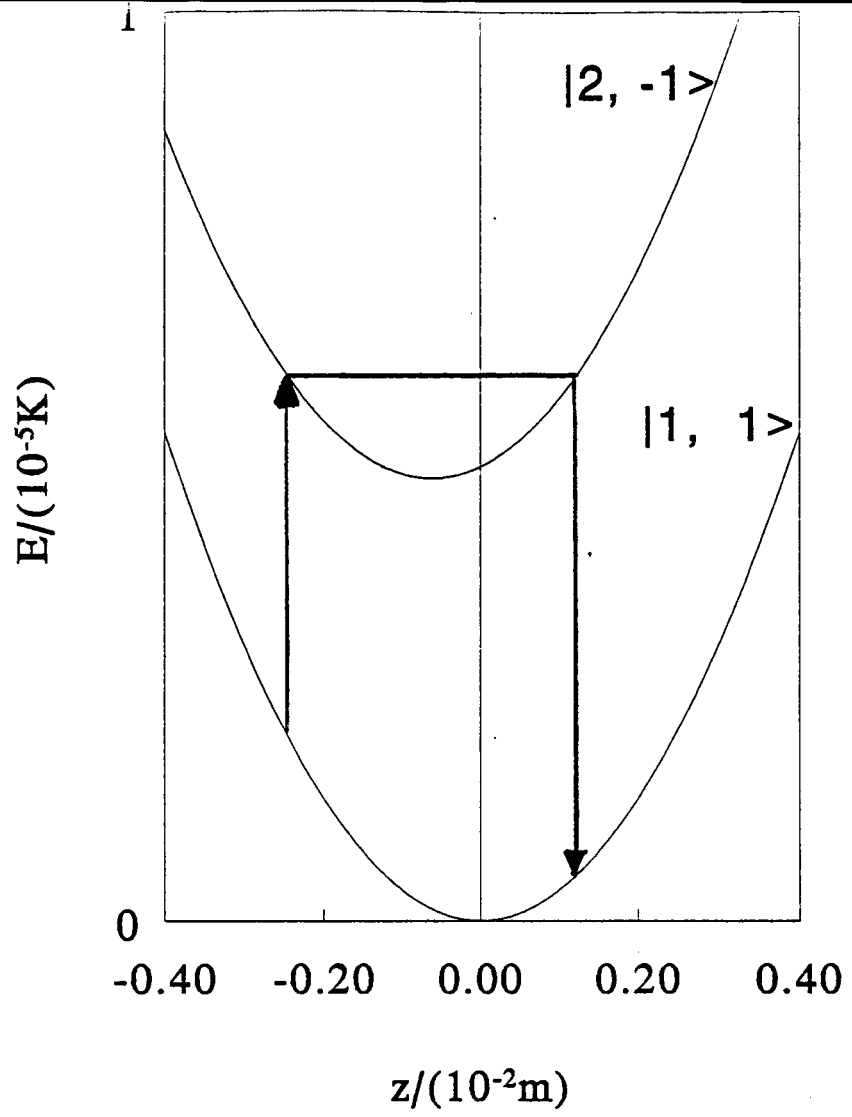

Figure 2.2: Total potential energy of the $|1,-1>$ and the $|2,1>$ states. The additional 0.328 mK offset of the $|2,1>$ state is not shown. The arrows indicate one cooling cycle, as explained in the text.

internal potential energy of the $|2,1>$ state due to the magnetic field gradient that cancels the force of gravity for the $|1,-1>$-state. The term mgz denotes the gravitational potential energy. The corresponding energy curves are shown in fig 2.2.

Clearly the positions of the minima of the corresponding energy curves do not coincide. The resulting shift, Δz,

$$\Delta z = \frac{16mg}{\beta\hbar}\left[\frac{\gamma_n}{(\gamma_e + 5\gamma_n)(\gamma_e - 3\gamma_n)}\right], \tag{2.8}$$

which for ^{87}Rb is of the order of $(6.2\ 10^{-4}/\beta)$ m, (β in Tm^{-2}), lays the basis for the gravitational Sisyphus cooling mechanism: atoms that are initially in the lower potential well are selectively excited at $z < 0$ to the $|2,1>$-potential, using a two-photon excitation. This can be accomplished e.g. by using micro-wave radiation to make the transition $|1,-1> \rightarrow |2,0>$, followed by absorption of rf radiation, inducing the transition $|2,0> \rightarrow |2,1>$.
After half an oscillation in the upper potential, at classical turning-point at $z > 0$ (right in figure), the atoms are de-excited into the lower potential well by pulsed optical pumping through the $P_{1/2}$ or $P_{3/2}$ states, in which process spontaneous emission occurs [14]. Note, however, that the atoms are now closer to the minimum of the $|1,-1>$-parabola than at the excitation. This means that the atoms in the de-excitation process loose *more* energy than they initially gained in the excitation process. Clearly this cycling between $|1,-1>$ and $|2,1>$ states leads to cooling of the atoms.
Using this method, atoms have been cooled in the vertical dimension to about 1.5μK [14]. Note, that although the atoms are cooled only in the vertical direction, elastic collisions cause equilibration of the temperature in all three directions. Thus, continuous cooling in the z-direction results in cooling in all three directions. The cross-section for elastic ground-state collisions between two $|1,-1>$-state atoms can be derived from the rethermalisation rate of the gas [15].

2.1.2 Rf-induced evaporative cooling

In this subsection we will discuss another novel cooling technique which is very promising for achieving very low temperatures: *rf induced evaporative cooling* of atoms. In this set-up, ^{23}Na atoms ($i = 3/2$) have been trapped in a dc magnetic field [16].
Figure 2.3 shows the potential energy of the $f = 1$-states in a configuration in which the dc magnetic field increases linearly with z, $B(z) = B_0 z$. By applying rf-radiation of frequency ω_{rf} one can make a "hole" in the trapping potential of the $|1, -1>$-state. For at the position z_h, defined by

$$\mu B(z_h) = \hbar\omega_{rf}, \tag{2.9}$$

(where $-\mu$ is the magnetic moment of the $|1, -1>$-state), the rf-radiation is resonant with the transition to the *non-trappable* $|1, 0>$ and $|1, 1>$ states. Thus at this particular magnetic field (i.e. at a certain z), the rf-radiation removes the atoms which are in resonance from the trap by spinflipping them to the non-trappable hyperfine states.

Clearly, the energy of the atoms that are removed from the trap can be varied by changing the rf-frequency. Thus, if the rf-frequency is tuned such that atoms with the highest energy are removed from the trap, after rethermalisation of the remaining atoms, the temperature of the gas is reduced. This motivates the term " rf-induced evaporative cooling". The cooling procedure can be repeated by decreasing the rf-frequency, so atoms that after rethermalisation have the highest energy can be extracted from the trap.
In recent experiments ^{23}Na atoms were trapped and cooled using the above-mentioned method and the temperature was observed to decrease by a factor of five at constant density [16].

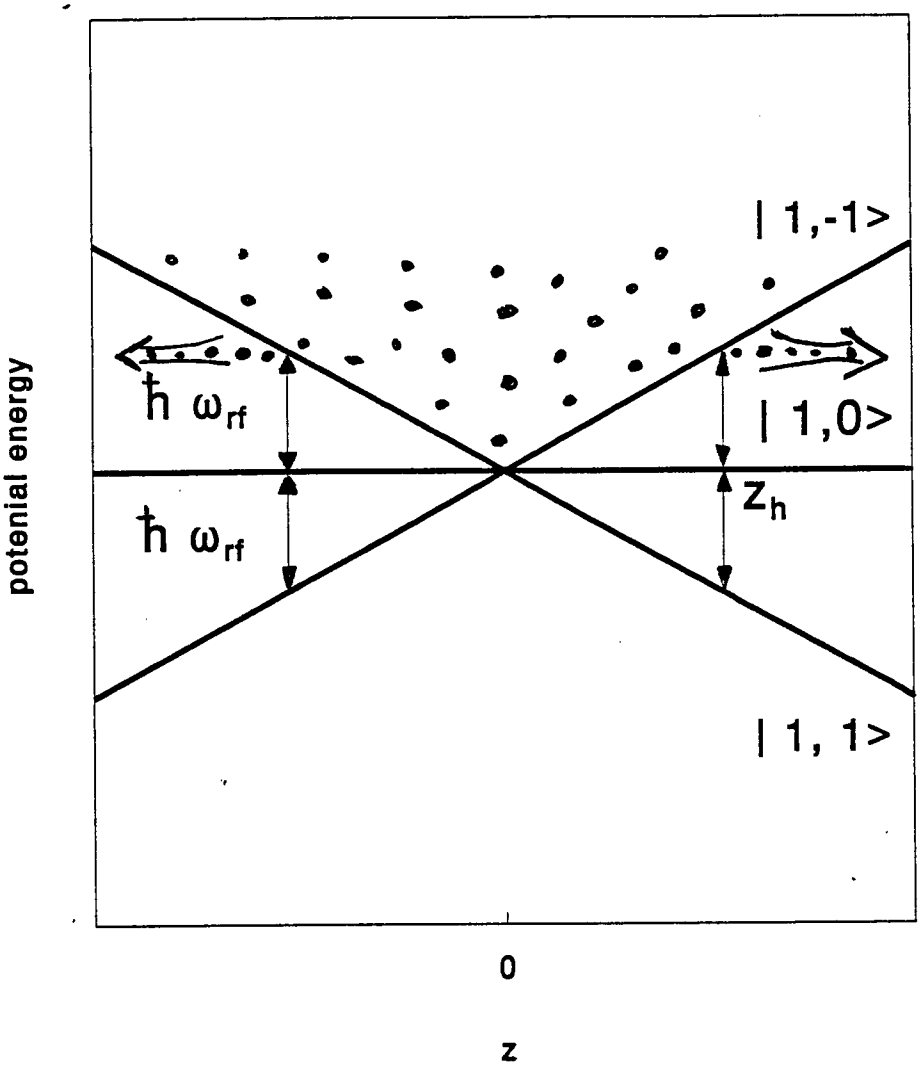

Figure 2.3: Potential energy of the $f = 1$ states in a magnetic field $B(z) = B_0 z$. At the position z_h the rf-radiation is resonant with the non-trappable hyperfine states. The atoms can leave the trap through the "hole".

2.2 Experimental setup of the FORT

The FORT uses optical methods to store atoms. It consists of a single linearly polarised focussed Gaussian laser beam that has a wavelength λ tuned between 4 and 67 nm to the red of the $S_{1/2} - P_{1/2}$ (D1)-transition of 795 nm [9]. The atoms in this beam are trapped by the so-called optical dipole force. To illustrate the operation of this optical dipole force, we consider a two-level atom of resonance (transition) frequency ω_0 in the field of a laser of frequency ω_L. The electric field $\vec{E}_L(\vec{r})$ of the laser induces an electric dipole moment in the trapped atoms. This, in turn, leads to a negative change in internal energy of the atom, proportional to E_L^2, which acts as a potential energy term on the atom. It thus experiences a *trapping force* directed to the focal point of the laser beam. The associated trapping potential U on the atom is given by [10]:

$$U = \frac{\hbar \Omega_R^2(\vec{r})}{4\Delta}, \tag{2.10}$$

where $\Omega_R = < \psi_e|\vec{d}|\psi_g > \cdot \vec{E}_L(\vec{r})/\hbar$ is the Rabi-frequency, ψ_g and ψ_e are the internal ground- and excited state wavefunctions, $\vec{d}$ is the atomic dipole operator and $\vec{E}_L(\vec{r})$ is the electric field of the laser, which is a function of the position $\vec{r}$; $\Delta = \omega_L - \omega_0$ is the laser detuning from atomic resonance.
In equation (2.10) we assumed that $\Delta >> \Omega_R$ and $\Delta >> \Gamma$ where Γ is the line width of the excited state.

The rate at which atoms spontaneously scatter (absorb and subsequently spontaneously emit) the laser photons, γ_s, is given by [11] :

$$\gamma_s = \frac{\Gamma \Omega_R^2}{4\Delta^2}. \tag{2.11}$$

The advantage of large detuning can now be seen from equations (2.10) and (2.11): Upon increasing the detuning Δ , we can get the *same trapping potential* when the laser intensity (prop. Ω_R^2) is increased simultaneously. Moreover, as can be seen from equation (2.11), the spontaneous scatter rate decreases so the heating due to recoil in spontaneous emission also decreases.

Another advantage of the large detuning in the FORT is the fact that unlike in usual optical traps (not far detuned), in which a large fraction of the confined ground-state atoms are pumped to an excited state, the collisions between ground- and excited state atoms are *minimised* in the FORT; the cross-section associated with these collisions is proportional to Ω_R^2/Δ^2 [12]. These collisions lead to heating of the trapped gas and to loss of atoms from the trap. Therefore the loss of atoms from the trap due to the *trapping laser* is drastically decreased in the FORT.

Typical parameter values at $\lambda = 814$ nm, $P = 0.8$ W and a waist of about 10 μm, are a trap depth of 6.0 mK and a photon scatter rate $\gamma_s = 4.0 * 10^2 s^{-1}$. The temperatures achieved in the FORT typically range from 0.5-2 mK [9]. As we shall see, the FORT is well suited for studying cold atomic collisions between ground and excited state atoms that

are induced by a second independent laser beam (the so-called catalysis beam). In the next chapter we will discuss these collisions and the way they can be used to determine ground-state potential parameters.

Chapter 3

Optical collisions

As was already mentioned in the introduction, it is our aim to improve the theoretical Rb_2 ground-state potentials using experimental information contained in trap-loss processes. In this chapter we will first discuss the "state of the art" Rb_2-ground-state potentials and introduce the parameters by which these potentials can be described. In the second section, we will motivate our choice to analyse first the data obtained in the FORT photo-association experiments by Heinzen et al., instead of the data from the MT. In the subsequent section, we will briefly go into some aspects of cold atomic collisions that take place in optical atom traps. We will confine our attention to so-called *optical collisions* that lead to loss of atoms from the trap. For a detailed and comprehensive discussion on optical collisions we refer to reference [17].

3.1 Rb_2 ground-state potentials

As a starting point for the calculation of atomic collisions, in principle we need to know the potential in detail over the whole interatomic range $R \in (0, \infty)$. In practice, however, the interatomic region can be divided into two intervals. At small internuclear distances the interaction between the atoms becomes very complicated and the potential is badly known. At large internuclear distances, the exact interaction between two ground-state atoms is much better known and can be given in terms of several (dispersion) parameters, depending on the particular colliding atoms.

3.1.1 Short range Rb_2-potentials

The only Rb_2 ground-state potential based on spectroscopic research (and consequently restricted to relatively small internuclear distances) that is known to us is the *singlet* potential obtained by Amiot [18]. This potential is obtained from extensive spectroscopic data using the inverse perturbation approach (IPA), and ranges from 6 to 21 a_0.
However, no *spectroscopic* Rb_2 triplet potential is known to us, so for the short-range

triplet potential we must use a theoretically calculated potential. The only triplet potential presently available is that of Krauss & Stevens who have theoretically calculated this potential in the range 7-20 a_0 [19]. Both potentials, including their long-range tail, are shown in fig 3.1 in the next subsection, from which it can be seen that the singlet potential has its mimimum near $R = 8$ a_0 and has a depth -0.018 a.u.; the triplet potential has its minimum at $R = 11.5$ a_0 and has a depth -0.0009 a.u., which is approximately 20 times less than the singlet minimum.

These curves yield reasonable starting potentials but at short range the singlet and triplet interactions are badly known. The influence of this part of the potential on the radial wavefuntion, however, can, for each energy E and rotational quantum number N, be accounted for by one parameter only, the accumulated phase ϕ at a certain distance R_0: ϕ_0. This accumulated phase essentially contains the "history" of the wavefunction due to the short-range potential in the region $R < R_0$. Therefore we need not know the detailed form of the short-range potential: changing the potential in the region $(0, R_0)$ is equivalent to changing the accumulated phase at R_0. The phase ϕ_0 depends on energy E and rotational angular momentum N. In section 3.5 we shall see that in practice ϕ_0 shows a linear dependence on E and $N(N+1)$ in the relevant range of E and N.

SUMMARIZING: knowledge of the exact form of the short-range potential behaviour is equivalent to knowledge of $\phi_0(N, E)$.

3.1.2 Intermediate and long-range Rb_2-potentials

At relatively large internuclear distances ($R > 20a_0$) the interaction between the two ground-state atoms is caused by the dispersion interaction and the exchange interaction V_{exch}. The well-known dispersion interaction arises from instantaneous fluctuations in the charge distribution of the two atoms. These fluctuations momentarily cause an electric dipole moment in the neutral atom. This in turn will induce a dipole moment in the other atom and the atoms will interact via the electric dipole interaction. Using second order time independent perturbation theory it can be shown that one finds in this way the $-C_6/R^6$ term representing the van der Waals interaction. Taking also higher multipoles and higher orders into account, one finds the exact form of the dispersion interaction

$$V(R) = -\sum_{n=3}^{\infty} \frac{C_{2n}}{R^{2n}}. \tag{3.1}$$

The exchange interaction arises from the gradual overlap of the two electron clouds when the atoms are brought together. Its tail is commonly taken to have the form

$$V_{exch}(R) = ae^{-bR}. \tag{3.2}$$

The singlet (S=0) and the triplet (S=1) interactions have the same long-range dispersion tail; the splitting between the two potentials is caused by the exchange interaction.

At "intermediate" and long-range distances the triplet(S=1)-potential is in good approximation given by

$$V_t(R) = -\frac{C_6}{R^6} - \frac{C_8}{R^8} - \frac{C_{10}}{R^{10}} + ae^{-bR}, \tag{3.3}$$

and the singlet(S=0)-potential by

$$V_s(R) = -\frac{C_6}{R^6} - \frac{C_8}{R^8} - \frac{C_{10}}{R^{10}} - ae^{-bR}. \tag{3.4}$$

We determine the exchange parameters a and b from the constraint that the short-range potentials must be connected differentiably to their short-range limits. However, we must first determine acceptable values for the dispersion coefficients C_6, C_8 and C_{10}. In the following table we have listed the most recent values for these dispersion coefficients.

reference	10^{-3} C_6 a.u.	10^{-5} C_8 a.u.	10^{-7} C_{10} a.u.
[31]	4.768	5.244	6.863
[30]	5.726	6.115	6.316
[32]	4.426	5.506	7.665
[33]	4.350		
[34]	4.700		

The values obtained by Marinescu ([32]) are believed to be most reliable. In view of the large scatter among the values reported in literature, we choose

10^{-3} C_6 a.u.	5.0 ± 0.7
10^{-5} C_8 a.u.	5.7 ± 0.5
10^{-7} C_{10} a.u.	7.5 ± 0.5

Using these values the individual dispersion terms at $R = 30\ a_0$ become

$$\begin{aligned} V_6 &= (6.86 \pm 0.96)\ 10^{-6} \text{ a.u.}, \\ V_8 &= (8.69 \pm 0.76)\ 10^{-7} \text{ a.u.}, \\ V_{10} &= (1.27 \pm 0.08)\ 10^{-7} \text{ a.u.}. \end{aligned} \tag{3.5}$$

Upon using the central values for C_6, C_8 and C_{10}, differentiable connection to the Krauss & Stevens triplet-potential results in

$$\begin{aligned} a &= 136.86 \text{ a.u.}, \\ b &= 0.8818\ \text{a}_0^{-1}, \end{aligned} \tag{3.6}$$

so the exchange potential at $R = 30\ a_0$ is $4.44\ 10^{-10}$ a.u., which is negligible compared to the dispersion terms.
In the long-range region where the photo-association occurs, the potentials can even be described by the C_6 and the C_8-terms only:

$$V(R) = -\frac{C_6}{R^6} - \frac{C_8}{R^8}. \tag{3.7}$$

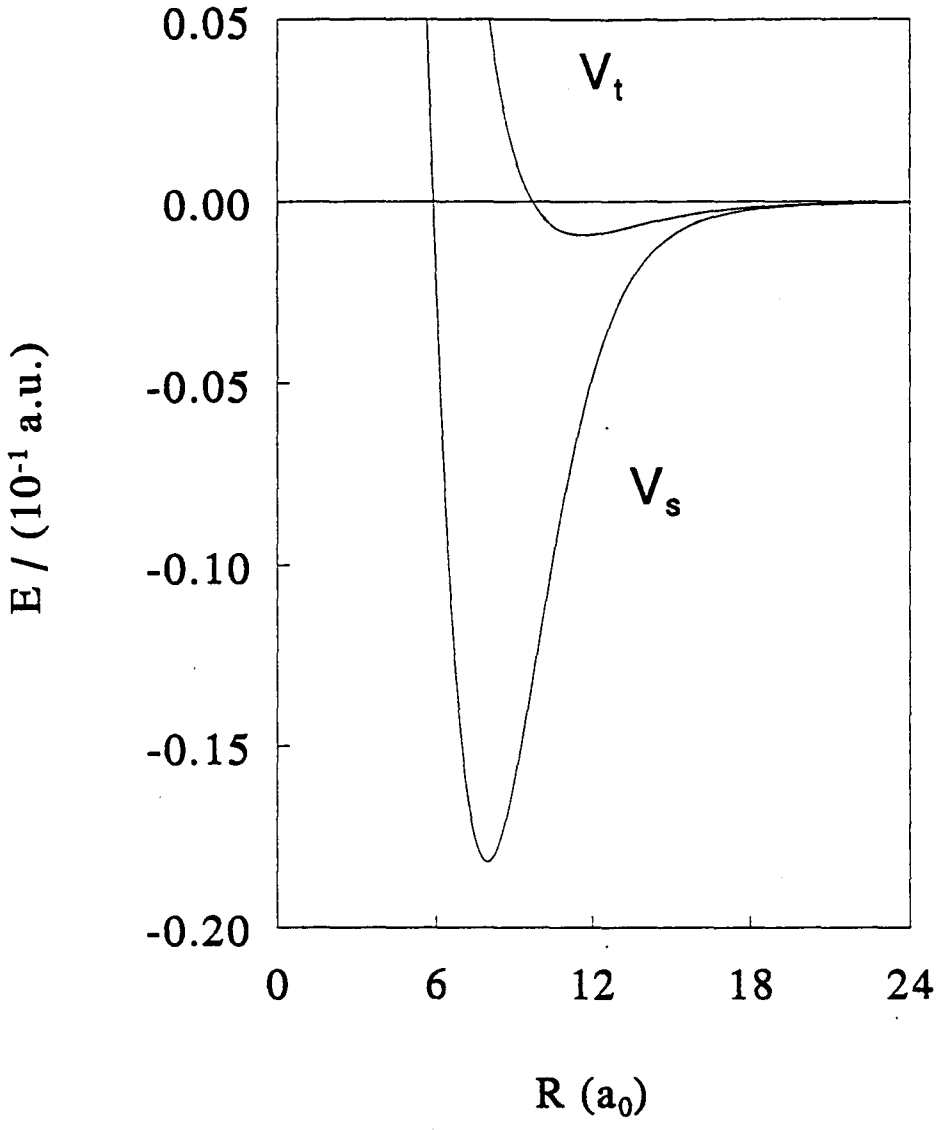

Figure 3.1: Rb_2 singlet and triplet potentials

3.2 Choice between the MT and the FORT

We now come to the choice between analysing MT or FORT-data. In the previous chapter we have discussed the trapping principles of the MT and the FORT. The collisional states are in principle always a mixture of both singlet and triplet components. Therefore in the analysis of the experimental data one must *simultaneously* take singlet and triplet parameters into account. This means that the parameters effectively describing the short-range potentials, that is $\phi_{0s}(N,E)$ for the singlet and $\phi_{0t}(N,E)$ for the triplet are involved in calculation of trap loss-processes. In addition to these short-range parameters, the "intermediate" exchange parameters a and b and the long-range dispersion coefficients C_6, C_8 and C_{10} must be taken into account in collisional calculations.
Thus as much as seven parameters must be determined as well as the distribution over the hyperfine ground-states contained in the initial state! If the Rb_2-potentials that we want to improve were reasonably well-known, implying "good" starting values for the above-mentioned parameters, there might have been a possibility to extract accurate parameter values from comparison of theoretical calculations and experiment. But even in that hypothetical situation we would have faced a Herculean task.

However, these problems can be overcome in the FORT if the experimental set-up is changed. If the ground-state atoms are continuously pumped into the (f, m_f)=(3,3) state, the nuclear and electronic spins are fully "stretched", i.e. $m_i = 5/2$ and $m_s = 1/2$. Because these so-called *doubly-polarised* atoms have the same projections of the electronic spin in the direction of the magnetic field, they can only interact via the triplet interaction. So within this experimental set-up the collisions are fully determined by the triplet potential. In the MT, however, the atoms can *not* be doubly-polarised so the collisional states always consist of a mixture of singlet and triplet states.

An additional advantage of the FORT is the fact that the trap-losses are *externally induced* by means of a laser that excitates the ground-state atoms to an excited state. When this state decays, the atoms predominantly leave the trap (see next section). This laser has a tunable frequency and this frequency *determines the internuclear distance at which the atoms make the transition* to the excited state. The laser frequency ω_L can even be chosen such that the transition occurs in the very long ground-state tail that is effectively described by C_6 only! This provides a very promising strategy to determine the ground-state parameters. Comparison of theoretical calculations with experimental data should yield an accurate value for C_6. Then ω_L is set to such value that the laser excitation occurs in the region of smaller internuclear distances where the ground-state potential is to a very good approximation determined by the dispersion coefficients C_6 and C_8. Since C_6 is "known", C_8 can now be determined. This strategy can then be repeated: working inwards, starting from large internuclear distances allows the determination of the required potential parameters.

We conclude that it is much more promising to analyse the trap-losses from the doubly-polarised atoms in the FORT. Our further discussion is therefore restricted to the analysis of the trap-loss mechanisms in the FORT.

3.3 Optical collisions: photo-association

In the preceding section we pointed out that it is possible to deduce the ground-state Rb_2-potential parameters from the experimentally measured loss of atoms from the FORT. But how can the FORT-experiment then be used to derive potential parameters if the main reason for far-off-resonance trapping is to *minimize* the loss of atoms from the trap?
The answer simply is: the actual atomic trap-loss is *not* induced by the FORT *trapping* laser (of constant frequency ω_t), but by a *second independent laser* of variable frequency ω_L. This laser will cause so-called optical collisions that give rise to the measurable loss of atoms from the FORT. Therefore we will now first discuss these important optical collisions.

A collision of two atoms (in presence of a laser field), one of which resonantly absorbs a laser photon during this collision, is called an *optical collision.* In the FORT for example we initially have two colliding ground-state atoms in the $S_{1/2} - S_{1/2}$-state. This colliding pair of atoms initially has an energy of the order of kT relative to the ground-state Rb_2 dissociation limit, where k is the Boltzmann constant and T denotes the temperature of the gas. During the collision, at a certain distance, the so-called Condon radius R_C, the laser field of frequency ω_L becomes resonant with the transition to an excited state.
At this resonant distance, the ground-state "molecule" can make an electric dipole transition to this excited state. In particular the ground-state can make a transition to a *bound* state of the excited potential

$$Rb + Rb + \hbar\omega_L \rightarrow (Rb + Rb^*), \tag{3.8}$$

which is called *photo-association.* This process is illustrated in figure 3.2. When ω_L is being changed, resonances will occur whenever $\hbar\omega_L$ matches the energy difference between the bound excited molecular states and the initially free state. It is of importance to emphasize the fact that the colliding atoms in the FORT are ultra-cold. The resulting energy spread of the initial collisional states is so small that the sharpness (resolution) of the free-bound absorption lines can be comparable to that of a transition between *two* bound states [20] ! Even rotational structure can be resolved.

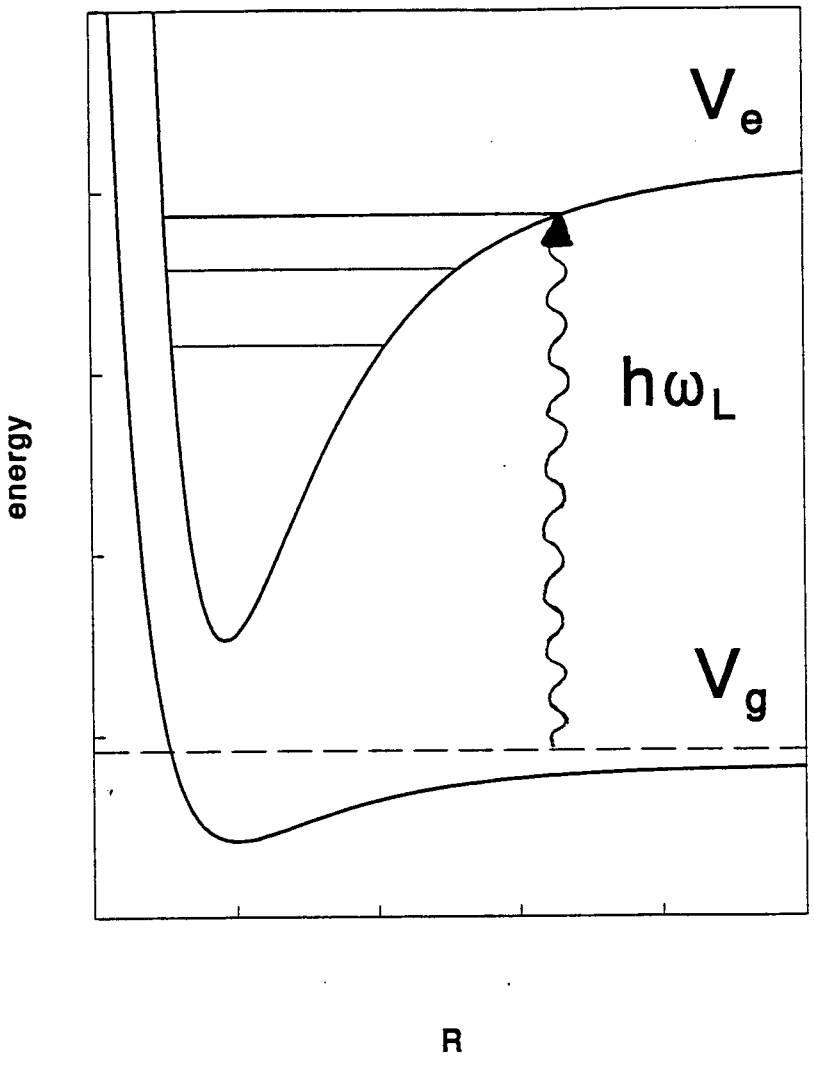

Figure 3.2: Schematic picture of the photo-association process. V_g and V_e are the ground and excited state potentials, respectively. The dashed line represents the initial energy of the colliding atoms. By absorption of a laser photon of energy $\hbar\omega_L$, the initial free state makes a transition to a bound state in the excited potential.

At the large internuclear distances ($R > 30a_0$) we are first interested in, the resonant distance R_C lies in the long-range potential part. Since the long-range van der Waals ground-state potential is negligible compared to the $-C_3/R^3$ tail of the excited state, the atoms constituting the excited molecule are rapidly accelerated towards each other and gain extra relative kinetic energy when the internuclear distance decreases.

Any subsequent spontaneous decay of the bound state to the ground-state, by emission of a photon, will generally lead to loss of the two atoms from the trap. This follows from conservation of energy: if we denote the energy of the emitted photon, which is a function of R, by $\hbar\omega_f(R)$ and the relative kinetic energy of the atoms in the initial ground-state and in the bound excited state by E_{k_i} and $E_{k_f}(R)$, respectively, then

$$E_{k_f}(R) + \hbar\omega_f(R) = E_{k_i} + \hbar\omega_L. \tag{3.9}$$

Thus the emitted photon is redshifted by an amount $\hbar\delta(R) = E_{k_f}(R) - E_{k_i}$, which increases as C_3/R^3. Therefore decay will predominantly occur to free states of much higher kinetic energy than the initial relative kinetic energy E_{k_i}. This increase in relative kinetic energy is divided among the two atoms and generally is large enough to let the atoms escape from the FORT, causing the above-mentioned trap-loss, as is illustrated in fig 3.3. Similarly, by emission of a photon of frequency $\omega_f > \omega_L$, the atoms decay into a *bound* Rb_2 ground-state molecule, which also results in loss of trapped atoms.

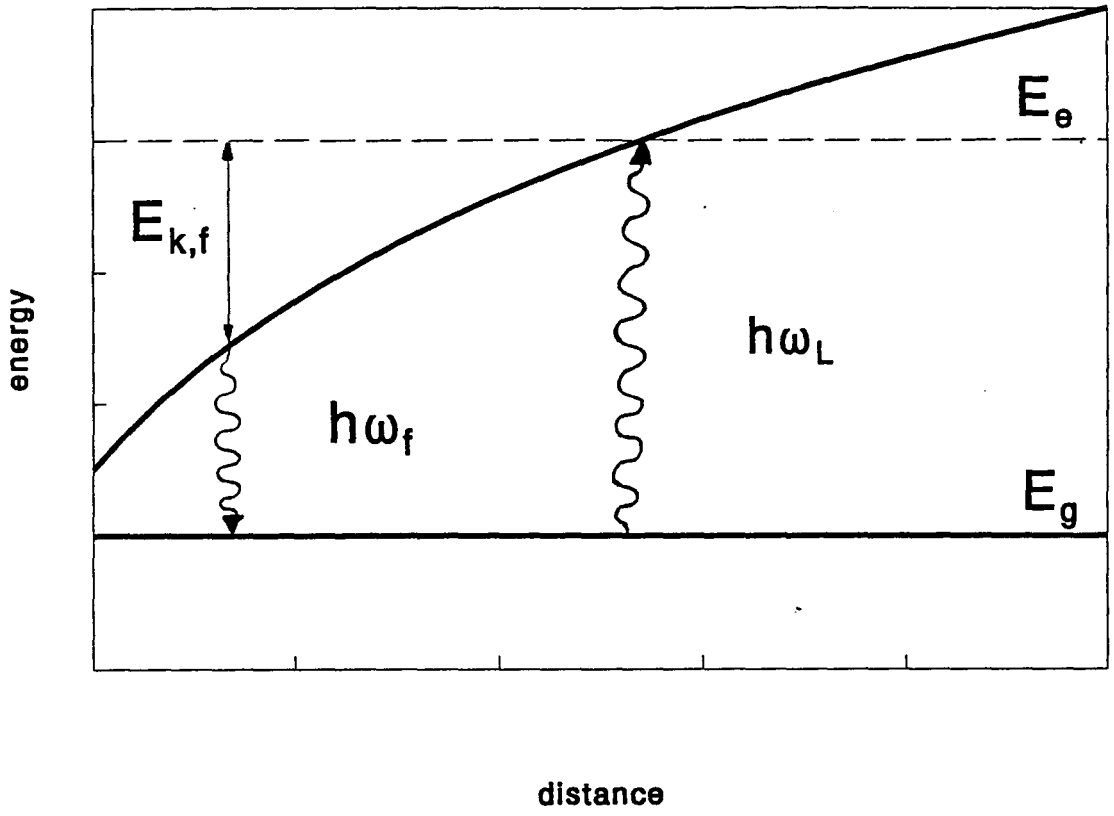

Figure 3.3: Schematic picture of the trap loss process, as described in the text. The ground-state potential V_g is taken to be zero; the excited state potential varies as $-C_3/R^3$. The relative kinetic energy in the ground-state is supposed to be negligible. The initial state absorbs a laser photon of energy $\hbar\omega_L$. Due to the rapid gain of relative kinetic energy of the atoms, however, the excited state emits a photon of energy $\hbar\omega_f < \omega_L$.

In the next section we will discuss the FORT-experiment by Heinzen et al. and discuss how the measured trap-losses can be used to derive ground-state potential parameters.

3.4 Experimental photo-association spectra

We shall now briefly discuss the experiments by Heinzen et al., in which ultracold ^{85}Rb-atoms are confined in a FORT. The photo-association is performed by the so-called photo-association laser (PAL), which has a tunable frequency ω_L. If the associated photon energy $\hbar\omega_L$ matches the energy difference between an excited bound state and the continuum ground-state, it is possible to have a transition to that bound excited state. The resulting photo-association spectrum may therefore be used to determine the positions of the bound excited states, as was first pointed out by Thorsheim, Weiner and Julienne [20].

In the experiment the photo-association beam is on for a time of 100 ms. After this time both the trapping laser beam and the PAL beam are turned off. The remaining atoms in the trap are then detected using laser-induced fluorescence. The measured fluorescence signal is proportional to the number of atoms probed, so this signal can be used to determine the amount of atoms left in the trap. The measured fluorescence signal is sometimes called the *photo-association spectrum.*

Obviously, when the PAL is tuned to a resonance, the fluorescence signal shows a dip. This can be seen from fig 3.4, obtained by Heinzen et al. [21]. It shows the fluorescence signal, obtained from photo-association near the $S_{1/2} - P_{1/2}$ dissociation limit, as a function of the PAL frequency ω_L. Note that the signal intensity is plotted to *increase downward*: the "upward peaks" therefore correspond to resonance transitions to bound excited states. The peaks shown in fig 3.4 correspond to resonance transitions to vibrational levels of the 0_g^- and 1_g potentials that asymptotically connect to the $S_{1/2} - P_{1/2}$ state.

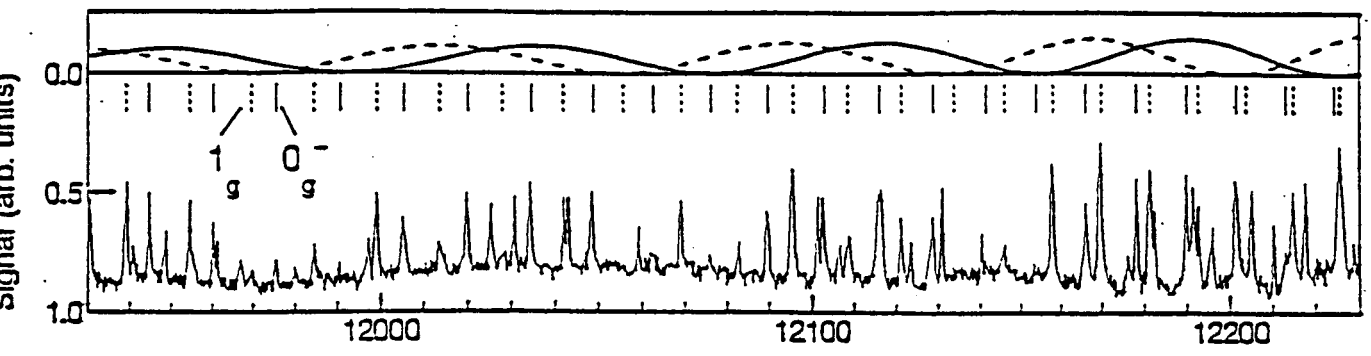

Figure 3.4: Photo-association spectrum of ultra-cold Rb atoms, obtained by Heinzen et. al.. The spectrum consists of two vibrational series corresponding to transitions to bound states in the 1_g (dashed vertical line above peaks) and in the 0_g^- (solid vertical line above peaks) states as a fuction of the PAL laser frequency (cm^{-1}). The inset shows the Franck-Condon oscillations

An important feature of the photo-association spectra is the oscillation of the intensity of the peaks, the so-called Franck-Condon oscillations, which is illustrated in the upper part of fig 3.4. This oscillation reflects the structure of the ground-state wavefunction as can be explained from a simplified but physically acceptable model, in which the excited state wave-function is concentrated near its outer classical turning point. By virtue of the Franck-Condon principle, the transition probability from the ground-state to the bound excited state is proportional to the product of the wavefunctions near the outer classical turning point of the bound (vibrational) level. If this turning point coincides with a node in the ground-state wavefuction the probability for transition to excited state will be very small. Therefore nodes in the ground-state wavefunction generate minima in the photoassociation spectrum. The Franck-Condon oscillations may therefore be used to determine the position of the nodes in the ground-state wavefunction. These in turn can be used to calculate the long-range ground-state potential parameters.

Upon resolving the vibrational peaks, they turn out to show an additional rotational structure. Essentially these rotational peaks are the convolution of the Lorentzian profile describing the resonance behaviour of the excited state with the initial velocity distribution over the ground-states and the associated transition matrix-element. Since the resulting shape is very sensitive to modifications in the ground-state potential, comparison of experimental and theoretical spectra evidently provides a way to determine the ground-state potentials most accurately.

In the next section we will discuss the behaviour of the ground-state wavefuction, which is of great importance in the analysis of the data from the FORT. In particular the dependence of the accumulated phase on the total energy and the relative orbital angular momentum is investigated.

3.5 Behaviour of the ground-state wavefunction

In order to extract accurate ground-state potential parameters from the experimental data, it is important to know the behaviour of the ground-state wavefunction as a funcion of energy E and relative orbital angular momentum N of the atoms. The position of the nodes in the ground-state wavefunction e.g. can be used to derive the ground-state dipersion coefficient C_6. Because the atoms in the trap are supposed to obey a Maxwell-Boltzmann energy distribution, and since the position of the nodes in the ground-state wavefunction depend on E, there is always a large range of allowed collision energies for which the resulting nodes in the ground-state wavefunction must be determined. Furthermore, we must also consider the influence of the relative atomic orbital momentum N, since the centrifugal barrier resulting from N also affects the position of the nodes in the ground-state wavefunction.

In order to determine the influence of fluctuations in E and N on the (position of the nodes in the) triplet ground-state wavefunction, we consider the dependence of the accumulated triplet phase ϕ_{0t} on these two parameters. For the change in the wavefunction caused by changing E and N is equivalently accounted for by the dependence ϕ_0 on E and N. This can be seen if we write the wavefunction in the JWKB-approximation. This JWKB-approximation is valid if the potential does not vary appreciably over the local wavelength of the ground-state wavefunction, i.e. everywhere except in the far dispersion tail. The wavefunction can then be approximated by:

$$\Psi(R) = A\frac{\sin(\phi + \phi_{0t})}{\sqrt{k}}. \tag{3.10}$$

Here A is a normalisation constant, $\phi(R) = \int_{R_0}^{R} k(R)dR$, is the accumulated triplet phase at internuclear distance R and $k(R) = \sqrt{\frac{2\mu}{\hbar^2}[E - V(R)]}$ is the R-dependent wavenumber, where E is the energy and $V(R)$ represents the total (=triplet + centrifugal) potential:

$$V(R) = V_t(R) + \frac{\hbar^2 N(N+1)}{2\mu R^2}. \tag{3.11}$$

Here N denotes the rotational quantum number.

The accumulated phase can be calculated from the value of the wavefuction and its derivative with respect to the internuclear distance (denoted by the primes):

$$\phi = \frac{\pi}{2} - \arctan(\frac{\psi'}{\psi} \cdot \frac{1}{k} + \frac{k'}{2k^2}). \tag{3.12}$$

This equation can be used to calculate the dependence of the accumulated triplet phase on E and N. To that end the short-range Rb_2 triplet potential $V_t(R)$ of Krauss & Stevens [19] was differentiably connected to the long-range tail for which the dispersion coefficients of [32] were used.

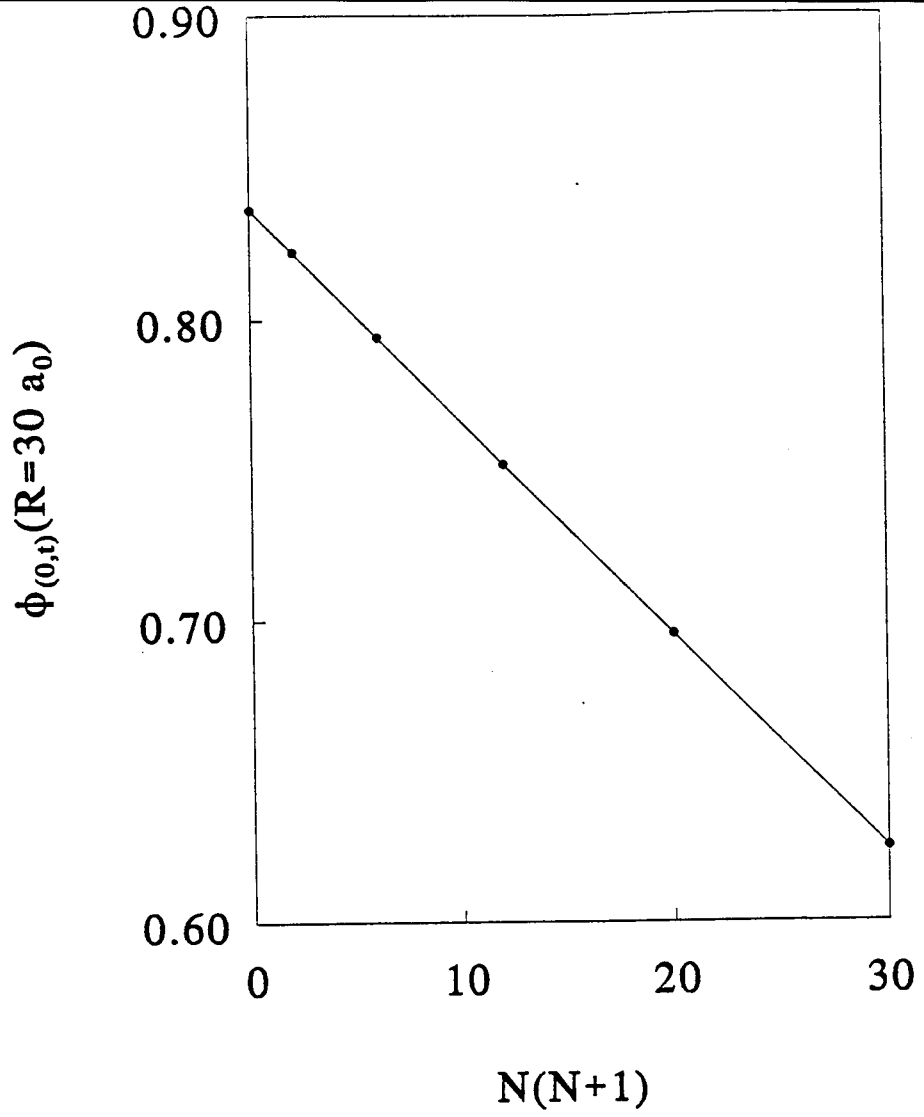

Figure 3.5: Accumulated triplet phase at $R = 30$ a_0 as a function of N(N+1)

We then numerically solved the radial Schrödinger-equation

$$(\frac{-\hbar^2}{2\mu}\nabla^2 + V_t(R) + \frac{\hbar^2 N(N+1)}{2\mu R^2})\Psi = E\Psi, \tag{3.13}$$

for several values of N and E.

The dependence of ϕ_{0t} on E and N was determined using equation (3.12). The results for the triplet phase at $R_0 = 30a_0$ are shown in the figures below.

From fig 3.5 it can be seen that the accumulated triplet phase ϕ_{0t} decreases linearly with N(N+1). This is a consequence of the centrifugal barrier that tends to push the wavefunction away from the origin, so at $R = 30a_0$ the wavefunction has completed less full oscillations (counted from R=0) than the wavefunction of the same energy corresponding to N=0.

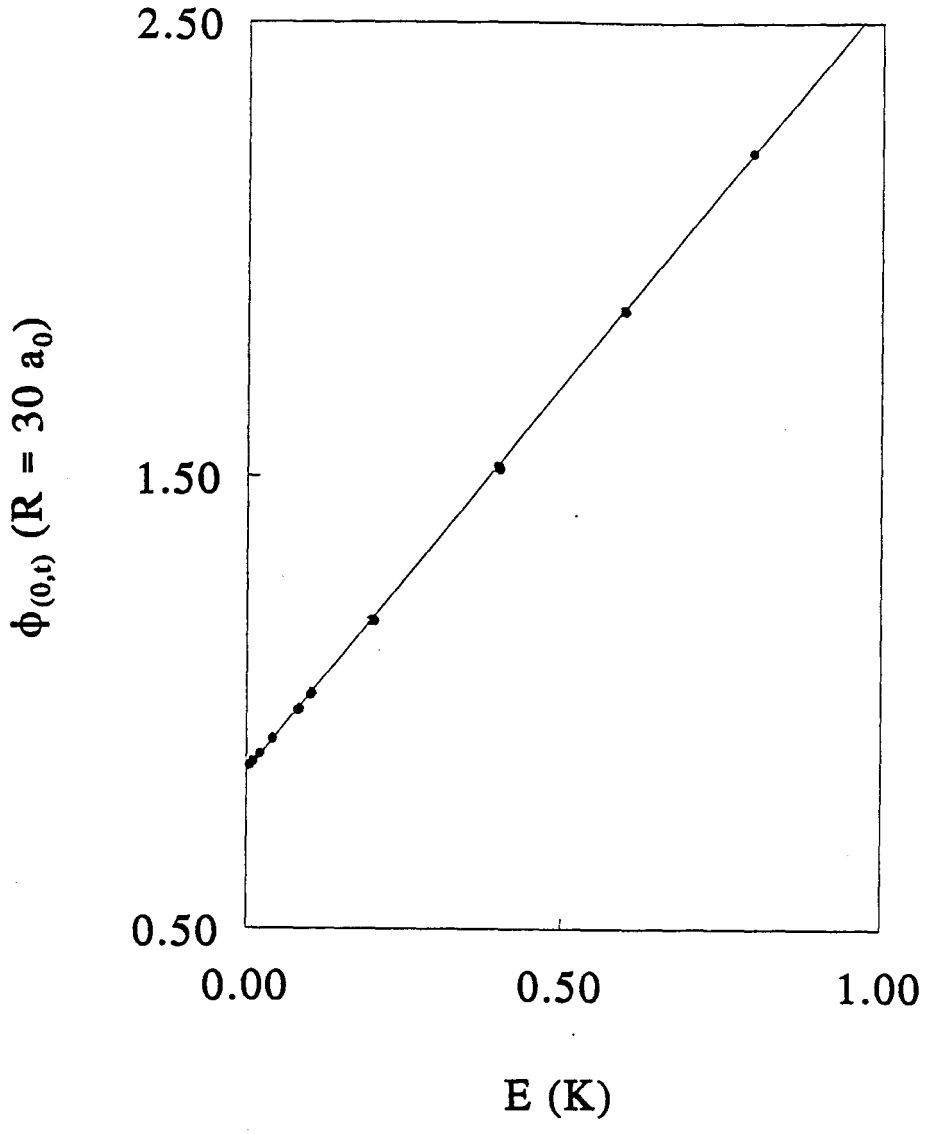

Figure 3.6: Accumulated triplet phase at $R = 30$ a_0 as a function of E

However, as can be seen from fig 3.6, the accumulated triplet phase increases linearly in energy when E increases: the wavenumber increases when E increases so the local wavelength decreases, thus at $R = 30a_0$ a wavefunction of higher energy has completed more oscillations than a wavefunction (of the same N) of less energy.

Since the temperature in the FORT appromimately is 1 mK and since only small rotational quantum numbers participate in the photo-association process, these figures show that both $\phi'_{Nt} := (\frac{\partial \phi_{0t}}{\partial (N(N+1))})|_{N=0}$ and $\phi'_{Et} := (\frac{\partial \phi_0}{\partial E})|_{E=0}$ are constant over the range that is of interest to us.

Therefore to an excellent approximation the dependence of the accumulated phase on energy and orbital angular momentum is given by

$$\phi_{0t}(N, E) = \phi_{0t}(0, 0) + N(N+1)\phi'_{Nt} + E\phi'_{Et}. \tag{3.14}$$

This equation confirms the statement in section 3.1 that the influence of the small-range potential part on the wavefuction is equivalently accounted for by the three parameters $\phi_{0t}(0,0)$, ϕ'_{Nt} and ϕ'_{Et} .

The prerequisites for the analysis of the experimental photo-association spectra are the atomic collisional model and accurate excited state potentials. These are the subjects of the next two chapters: in chapter 4 we will introduce an appropriate set of basis states for the characterisation of the collision. In chapter 5 we will calculate the potentials of the excited states involved in the optical collisions.

Chapter 4

Rotating diatomic molecules

In this chapter we will discuss some aspects of diatomic molecules that lay the foundation for the description of optical collisions. These include the connection between space- and molecule-fixed molecular states and the derivation of anomalous commutation rules for the *total* angular momentum with respect to the molecular frame. At the end of this chapter we will introduce the "generalised" kets that we use as the basis set the state-vector of the diatomic molecule. To avoid confusion, we will first define the coordinate systems we use and derive the connection between them.

4.1 Space- and molecule-fixed frames; Eulerian angles

There are two coordinate systems that are particularly useful in the description of atomic collisions: the space-fixed (x,y,z)-frame and the molecule-fixed (ξ, η, ζ)-frame. The space-fixed frame does not change its orientation in time, the molecule-fixed frame is anchored to the molecule. If the molecule rotates, the orientation of the molecule-fixed frame with respect to the space-fixed system changes. The origin of both frames is chosen to be the midpoint of the line joining the two identical nuclei. This means that the origin coincides with the center of mass. The orientation of the molecule-fixed frame with respect to the space-fixed system can be given in terms of the three Eulerian angles α, β, γ [22]. Their definition in literature greatly varies, so in order to prevent confusion we shall now explicitly define them. We suppose that the two frames initially coincide, the internuclear axis directed along the z-axis. Starting from this configuration we then perform the following three rotations:

- first we rotate the molecule-fixed frame through γ around the z-axis
- then we rotate the molecular frame through β around the space-fixed y-axis
- finally we rotate the molecular frame through α around the space-fixed z-axis.

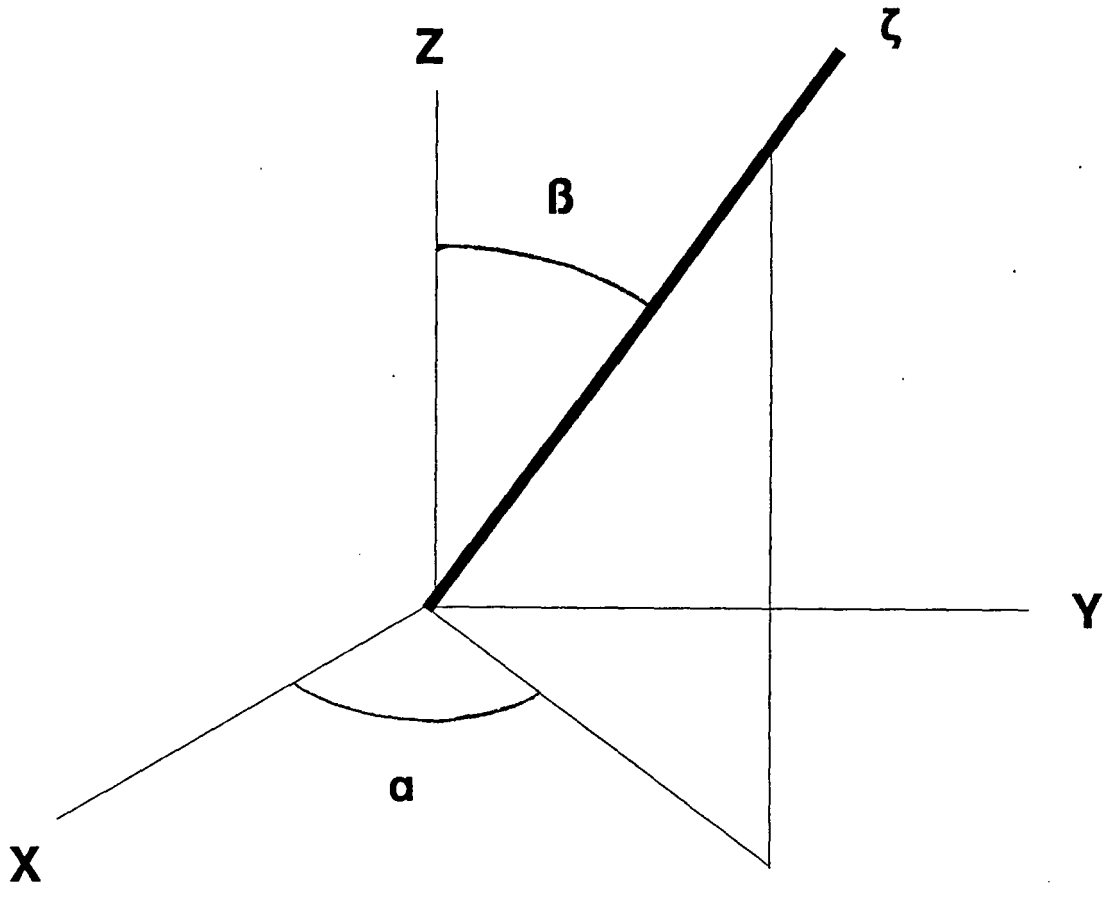

Figure 4.1: Orientation of the internuclear axis after rotation through the Eulerian angles as indiciated in the text.

The resulting orientation of the internuclear axis (with respect to the space-fixed system) is shown in fig 4.1 below. Note that α and β equal the familiar polar angles ϕ and θ of the internuclear axis, respectively.

4.2 Transformation of electronic states.

In collision calculations, molecular states are mostly implicitly defined with respect to the molecular frame because the symmetry labels that identify these states are related to symmetry operations in the molecular frame. In the experiment however when the distribution of the atoms over the different states is specified, these states are (nearly) always supposed to be defined with respect to the space-fixed (laboratory) frame. For example in the case of doubly-polarised atoms, the projection of the spins of the atoms is known with respect to a space-fixed direction, determined by the direction of the magnetic field by which the spins are oriented. The same is true for the laser polarisation that

induces the photo-association. It is therefore necessary to be able to switch between the two descriptions used. The transformation that allows us to express a space-fixed defined state in terms of its molecule-fixed defined equivalent and vice versa is easily obtained if we consider the behaviour of an electronic state under *active* rotations. These *active* rotations rotate the *shape* of the wavefuntion.

Let us start with an (atomic) electronic state with total angular momentum quantum number j and projection $m\hbar$ on the space-fixed z-axis, denoted by $|jm;z>$. In this notation the "z" explicitly reminds us of the fact that the state is defined with respect to the space-fixed coordinate system. An active rotation through Eulerian angles (α, β, γ) transforms this state into

$$e^{\frac{-i\alpha j_z}{\hbar}} e^{\frac{-i\beta j_y}{\hbar}} e^{\frac{-i\gamma j_z}{\hbar}} |jm;z>, \tag{4.1}$$

where $\hat{j}_z$ and $\hat{j}_y$ are the generators of infinitesimal active rotations around the space-fixed z- and y-axis, respectively. Upon multiplication with the unit operator

$$1 = \sum_{j,m'} |jm';z><jm';z|, \tag{4.2}$$

(4.1) transforms into

$$\begin{aligned} &\textstyle\sum_{m'} \; < jm';z|e^{\frac{-i\alpha j_z}{\hbar}} e^{\frac{-i\beta j_y}{\hbar}} e^{\frac{-i\gamma j_z}{\hbar}} |jm;z> \otimes |jm';z> = \\ &\textstyle\sum_{m'} \; D^j_{m'm}(\alpha,\beta,\gamma)|jm';z>, \end{aligned} \tag{4.3}$$

where we made use of the famous Wigner-D-functions.
From this we immediately obtain:

$$|jm;\zeta> = \sum_{m'} D^j_{m'm}(\alpha,\beta,\gamma)|jm';z>, \tag{4.4}$$

in which $|jm;\zeta>$ is an electronic state with quantumnumbers j and m *defined with respect to the molecule-fixed frame.* The inverse transformation that expresses a state $|jm;z>$ in its equivalent linear combination of states defined with respect to the molecule-fixed frame, is found using the unitarity of the D-functions:

$$|jm;z> = \sum_{m'} D^{j^*}_{mm'}(\alpha,\beta,\gamma)|jm';\zeta> \tag{4.5}$$

The above two definitions, lay the basis for transformation of molecular states whenever we must switch between space- and molecule-fixed descriptions.

4.3 Commutation rules for the total angular momentum.

In connection with our particular choice of basisfunctions for diatomic molecules in the next section, it will prove useful to consider the commutation rules for the *total* angular momentum of the diatomic molecule. However, we will firstly explain the notation we use throughout this report.

4.3.1 Notation.

In order to avoid lenghty explainations of the symbols in every following formula and for the sake of reference, we supply the following table of frequently used symbols:

- $\vec{\mathrm{L}}$ denotes the total electronic *orbital* angular momentum; its component on the space-fixed z-axis is denoted by M_L, its component on the ζ-axis is Λ.
- $\vec{\mathrm{S}}$ denotes the total electronic spin; its component on the space-fixed z-axis is M_S and the component on the ζ-axis is Σ
- $\vec{\mathrm{J}}$ is the total electronic spin $\vec{\mathrm{J}} = \vec{\mathrm{L}} + \vec{\mathrm{S}}$. Its component on the space-fixed z-axis is denoted by M_J and its component on the ζ-axis is Ω.
- $\vec{\mathrm{N}}$ is the relative orbital angular momentum of the atoms; its component on the space-fixed z-axis is M_N . Its component on the ζ- axis vanishes identically.
- $\vec{\mathrm{P}}$ is the total angular momentum of the molecule: $\vec{\mathrm{P}} = \vec{\mathrm{N}} + \vec{\mathrm{J}}$. Its component on the space-fixed z-axis will be denoted by M_P; its component on the ζ-axis is Ω.

4.3.2 Anomalous commutation rules

In connection with the analysis of the collision process of two atoms, one encounters a peculiar ("anomalous") commutation relation for the *molecule-fixed components of the total angular momentum* $\vec{\mathrm{P}}$. This results in the unusual property that the effect of the associated ladder operators is reversed compared to the space-fixed ladder operators. Since these ladder operators appear in the coupled channels equations (which will be derived in section 5.7), we will discuss them here. In the second part of this section we will demonstrate that the molecule-fixed components and the space-fixed components of the total molecular angular momentum, in particular the operators $\hat{P}_\zeta$ and $\hat{P}_z$, commute; this latter property is of *fundamental interest* in the construction of basis kets for the diatomic states.

In order to derive the anomalous commutation rules using a geometrical argument, we consider the effect of active rotations on a vector. Since the operators $\hat{P}_x$ and $\hat{P}_y$ generate active rotations about the space-fixed x- and y-axis, the effect of $[\hat{P}_x, \hat{P}_y]$ can be determined

from the behaviour of a solid body under rotations. If the rotations are performed with respect to space-fixed axes, it can easily be seen that

$$[\hat{P}_x, \hat{P}_y] = i\hbar\hat{P}_z, \tag{4.6}$$

in accordance with the *usual* commutation rules. But in the molecule-fixed frame the components $\hat{P}_\xi, \hat{P}_\eta$ and $\hat{P}_\zeta$ do not obey (4.6). To see this, we consider the behaviour of a vector $\vec{V}$ with components V_ξ, V_η and V_ζ under active rotations with respect to the molecular frame. We first rotate the vector $\vec{V}$ through α about the η-axis, changing $\vec{V}$ into $\vec{W}$. Thus the components of $\vec{W}$ with respect to the *initial* orientation of the molecular frame is different from those of $\vec{V}$ with respect to this frame. But now comes the trick! The second rotation though β about the ξ-axis is to be performed about the *new* ξ-axis because the frame is anchored to the vector. Moreover the *numerical values* of the components of the vector $\vec{W}$ with respect to the (simultaneously rotated) molecular frame are V_ξ, V_η and V_ζ. If we subtract from the resulting vector the vector that is obtained form reversing the order of the rotations, then simple matrix-calculation shows that the commutator $[R_\xi(\beta), R_\eta(\alpha)] = R_\zeta(-\alpha\beta) - 1$, where the R's denote rotation operators. This equation implies that the vector $R_\xi(\beta)R_\eta(\alpha)\vec{V}$ can be obtained from the vector $R_\eta(\alpha)R_\xi(\beta)\vec{V}$ upon rotating the latter through $-(\alpha\beta)$ about the ζ-axis. However, if the rotations had been performed with respect to the space-fixed system (i.e. $\xi \rightarrow$ x, $\eta \rightarrow$ y and $\zeta \rightarrow$ z), then the vector $R_x(\beta)R_y(\alpha)\vec{V}$ would have been obtained from the vector $R_y(\alpha)R_x(\beta)\vec{V}$ upon rotating the latter through $+\alpha\beta$ around the z-axis. This means that the sense of the rotation is reversed! Therefore the commutation relations for the components of total angular momentum $\vec{P}$ in the molecular frame become "anomalous":

$$[\hat{P}_\xi, \hat{P}_\eta] = -i\hbar\hat{P}_\zeta. \tag{4.7}$$

The anomalous commutation rules also imply anomalous ladder operators:

$$\begin{aligned} \hat{P}_+ &= \hat{P}_\xi + i\hat{P}_\eta \text{ decreases } \Omega \text{ by } 1 \\ \hat{P}_- &= \hat{P}_\xi - i\hat{P}_\eta \text{ increases } \Omega \text{ by } 1. \end{aligned} \tag{4.8}$$

Let us now show that $[\hat{P}_z, \hat{P}_\zeta] = 0$. To do so, again we consider the effect of rotations on a solid body with some body-fixed axis (for example a knitting pin piercing a potato). The result obtained from a rotation about the space-fixed z-axis through, say α, followed by a rotation through β about the body-fixed axis is indistinguishable from the result gotten by interchanging the order of the rotations. This simple argument yields the above-mentioned very important result:

$$[\hat{P}_z, \hat{P}_\zeta] = 0. \tag{4.9}$$

Obviously, equation (4.9) allows for the construction of molecular basis states with well-defined projections on both the molecular and space-fixed frames *simultaneously*!
In view of the foregoing discussion one might be tempted to think that all body-fixed angular momenta obey anomalous commutation rules e.g. $[J_\xi, J_\eta] = -i\hbar J_\zeta$.

However, this is not so! Except for the total angular momentum $\vec{P}$, all other angular momenta obey normal commutation rules because they do not change the orientation of the molecular frame, thus e.g.:

$$[\hat{J}_\xi, \hat{J}_\eta] = +i\hbar\hat{J}_\zeta. \tag{4.10}$$

4.4 Basis kets for rotating diatomic molecules

Since there is no prefered direction in space, the total angular momentum $\vec{P}$ and its projection P_z are conserved. Moreover $[P_z, P_\zeta] = 0$ (see equation (4.9)) so M_P and Ω can simultaneously be used within one ket. We are therefore led to define basiskets which we shall denote by $|J\Omega P M_P>$. Note that neither z, nor ζ appear in this notation; indeed this reminds us of the "mixed" character of the states: Ω is the projection on the ζ-axis, while M_P is the projection on the z-axis of $\vec{P}$.
So these kets specify the total angular momentum quantum number P of the molecule and its projections on the space-fixed z-axis and on the internuclear axis; the particular orientation of the molecule in space is specified by their dependence on the Eulerian angles; the information about the electronic configuration is contained in the total electronic angular momentum J and its projection on the internuclear axis, Ω. The explicit form of these "generalised" kets is given by [23]

$$|J\Omega P M_P>:= \sqrt{\frac{2P+1}{8\pi^2}} D^{P*}_{M_P\Omega}(\alpha,\beta,\gamma) \otimes |J\Omega;\zeta> . \tag{4.11}$$

The complex conjugate Wigner-D-functions satisfy:

$$\begin{aligned} \hat{\vec{P}}^2 \{D^{P*}_{M_P\Omega}(\alpha,\beta,\gamma)\} &= \hbar^2 P(P+1)\ D^{P*}_{M_P\Omega}(\alpha,\beta,\gamma), \\ \hat{P}_z\{D^{P*}_{M_P\Omega}(\alpha,\beta,\gamma)\} &= \hbar M_P\ D^{P*}_{M_P\Omega}(\alpha,\beta,\gamma), \\ \hat{P}_\zeta\{D^{P*}_{M_P\Omega}(\alpha,\beta,\gamma)\} &= \hbar\Omega\ D^{P*}_{M_P\Omega}(\alpha,\beta,\gamma). \end{aligned} \tag{4.12}$$

The kets (4.11) constitute a convenient set of basisstates at relatively small internuclear distances: the interatomic interactions are strong in this region and the angular momenta will couple to the internuclear axis. It is then appropriate to consider the internuclear axis as axis of quantisation. At very large internuclear distances however, the "molecule" essentially consists of two separate atoms and there is hardly any interaction between them. Consequently the angular momenta no longer couple to the internuclear axis so this axis looses its physical meaning as axis of quantisation. The physically appropriate states then are uncoupled states that have the space-fixed z-axis as axis of quantisation. These uncoupled states are products of electronic states $|JM_J;z>$ and the nuclear rotational eigenfunctions $|NM_N;z>$. These products can be coupled to states of total molecular angular momentum P:

$$|(JN)PM_P;z> = \sum_{M_J,M_N} < JM_JNM_N|PM_P > |JM_JNM_N;z>. \tag{4.13}$$

The distance where it is physically more approriate to switch from the space-fixed basis-states to molecule-fixed basis-states can be defined by the so-called *locking-radius* R_L [24]. We will come back to this point in chapter 5 when we discuss the influence of non-adiabatic coupling terms.

Summarizing: at small internuclear distances $|J\Omega PM_P>$ provides a good basis while at large internuclear distances $|(JN)PM_P;z>$ is physically more appropriate to specify molecular states. Of course, from the mathematical point of view both sets are equivalent. Needless to say, we will often have to perform the transformation between the two bases $|J\Omega PM_P>$ and $|(JN)PM_P;z>$. The required transformation can be obtained upon using the properties of Clebsch-Gordan coefficients and of Wigner-D-functions; we shall here only give the final results [23]

$$|J\Omega PM_P>=(-1)^{J-\Omega}\sum_N < J-\Omega P\Omega|N0>|(JN)PM_P;z> \tag{4.14}$$

and the inverse is given by

$$|(JN)PM_P;z>=\sum_\Omega(-1)^{J-\Omega} < J-\Omega P\Omega|N0>|J\Omega PM_P> . \tag{4.15}$$

Now that we are finally equipped with two appropriate sets of basisstates for diatomic molecules, we can go over to the determination of the symmetry properties of these states. Furthermore, we can now calculate the potentials of excited states of alkali-dimers that are needed in the calculation of optical collisions.

Chapter 5

Molecular potential curves for alkali dimers

In this chapter we shall discuss the molecular potentials that are of interest in optical collisions. These are the potentials between two ground-state atoms ($A + A$) and those between an excited and a ground-state atom ($A + A^*$). We are only interested in the application to Rb-collisions but because essentially the interaction between two identical alkali-atoms is the same, we confine our attention to the "model-alkali" A.

5.1 The Born-Oppenheimer approximation.

For thermal and cold collisions, the atomic velocities are almost negligible compared to the electronic velocities. Thus the timescale for the atomic collision is very large compared to the timescale of electronic processes. Therefore the electrons adapt themselves more or less adiabatically to the slow nuclear motion: we can visualise the electronic wavefunction to be anchored to the nuclei, forced to make the same rotations as the nuclei do. This picture allows us to refer the electronic wavefunction to the internuclear axis rather than to the space-fixed system. In essence this is the famous Born-Oppenheimer approximation [25], in which the electronic wavefunction Ψ is solved within the molecular frame, the nuclei supposed fixed. Thus we have to solve:

$$\{-\frac{\hbar^2}{2m}\sum_i \nabla_i^2 + V(\vec{r},\vec{R})\}\Psi(\vec{r};\vec{R}) = E(\vec{R})\Psi(\vec{r};\vec{R}), \tag{5.1}$$

in which i runs over all electrons and V represents the interaction potentials between all electrons and nuclei, depending on all electroncoordinates $\vec{r}$ and on the internuclear vector $\vec{R}$. Note that both the eigenvalue E and the eigenvector Ψ are parametric functions of $\vec{R}$.

Subsequently the motion of the nuclei is calculated using the electronic eigenvalue $E(\vec{R})$ as an additional potential term, giving rise to the total wavefunction $F(\vec{R})\Psi(\vec{r};\vec{R})$, in which

the "nuclear" wavefunction $F(\vec{R})$ satisfies the equation:

$$\{-\frac{\hbar^2}{2\mu}\Delta_R + E(\vec{R})\}F(\vec{R}) = EF(\vec{R}), \tag{5.2}$$

where E denotes the total energy. The approximation made in this way is the neglect of terms in the Schrödinger equation arising from the operation of the nuclear kinetic energy operator on the parametric dependence of the electronic wavefunction. What can be "cheaply" included in (5.2) is the so-called adiabatic correction energy, i.e. the expectation value of the ∇_R-term in the electronic state. This leads to the so-called adiabatic Born-Oppenheimer approximation.

Note that the Born-Oppenheimer approximation is expected to break down near values of $\vec{R}$ where the distance of two eigenvalues of $E(\vec{R})$ (corresponding classically to an electronic eigenfrequency) is small relative to a typical nuclear frequency. In the case of such an avoided crossing one has to solve a coupled set of equations, rather than a single one like (5.2).

5.2 Interactions between ground-state atoms

The ground-state "molecule" constisting of two ground-state atoms is effectively described by the Hamiltonian:

$$\hat{H} = \hat{T} + V_c(R) + \sum_{k=1}^{2} \hat{H}_k^{hf} + \sum_{k=1}^{2} \hat{H}_k^{Z}, \tag{5.3}$$

in which $\hat{T}$ is the kinetic energy operator, $V_c(R)$ represents the central interaction, $\hat{H}_k^{hf}$ is the hyperfine interaction in atom k and $\hat{H}_k^{Z}$ is the Zeeman interaction. The central interaction corresponds with the electronic energy $E(\vec{R})$ of equation (5.2) and embodies the influence of all Coulombic interactions between the neutral ground-state atoms. It is given by

$$V_c(R) = \sum_{\alpha=s}^{t} V_\alpha(R) |\alpha><\alpha|, \tag{5.4}$$

where $V_s(R)$ and $V_t(R)$ are the singlet and triplet potentials respectively, that were introduced in chapter 3, and $|\alpha><\alpha|$ are the corresponding projection operators.
The hyperfine interaction accounts for the interaction between the electronic and nuclear spin *within* one atom. In the case of a ground-state atom, the only non-vanishing contribution stems from the so-called Fermi-contact term:

$$\hat{H}_k^{hf} = \frac{a}{\hbar^2} \vec{s}_k \cdot \vec{i}_k, \tag{5.5}$$

in which $\vec{s}_k$ and $\vec{i}_k$ are the (valence) electronic and nuclear spin of atom k and the constant a determines the splitting of the hyperfine levels in zero magnetic field. As can be seen from this equation, the hyperfine interaction is invariant under simultaneous rotations of $\vec{s}_k$ and $\vec{i}_k$ and consequently conserves the total atomic spin $\vec{f}_k = \vec{s}_k + \vec{i}_k$ and its projection on an arbitrary axis, e.g. the internuclear axis. This term can therefore be written as:

$$\hat{H}_k^{hf} = \sum_{f,m_f} \frac{a}{2}[f(f+1) - i(i+1) - s(s+1)] |(si)fm_f;\zeta><(si)fm_f;\zeta|. \tag{5.6}$$

The last term in (5.3) represents the Zeeman interaction that describes the interaction of the atomic spins with an external magnetic field $\vec{B}$.

$$\hat{H}_k^{Z} = (\gamma_e \vec{s}_k - \gamma_n \vec{i}_k) \cdot \vec{B}. \tag{5.7}$$

Here γ_e and γ_n denote the gyromagnetic factors of the valence electron and the nucleus respectively. Because the magnetic field in the FORT is very weak, the Zeeman-term can safely be neglected.

For very large internuclear distances, the central interaction $V_c(R)$ becomes negligible compared to the atomic hyperfine interaction and the asymptotic atomic eigenstates then are the atomic hyperfine eigenstates. For ^{85}Rb, the total atomic spin f can take the values 2 and 3. The asymptotic molecular ground-states therefore are linear combinations of the

combinations of atomic total spins (f_1, f_2) = (2,2), (2,3) and (3,3). The asymptotic energy difference ΔE between these states is $3a$. The relative importance of the hyperfine interaction compared to the central interaction clearly depends on the internuclear distance between the atoms and can be estimated by comparing ΔE and the energy-difference between the singlet- and triplet potentials (i.e. the exchange energy): when $\Delta E << 2V_{exch}(R)$, the influence of the hyperfine interaction reduces to a constant offset with respect to the singlet and triplet curves. At internuclear distances where $\Delta E \sim V_{exch}(R)$, however, the role of $\hat{H}^{hf}$ becomes very prominent: the potentials show avoided crossings in this region and the hyperfine interaction causes coupling of the asymptotically different hyperfine eigenstates [26]. When the atoms are *doubly-polarised* however, (f, m_f) can only be (3,3) or (3,-3). In this situation (doubly-polarised atoms) we only have triplet scattering states and the influence of the hyperfine interaction reduces to a constant offset. The Hamiltonian (5.3) in that case simplifies to:

$$\hat{H} = \hat{T} + V_t(R) + \frac{5a}{2}. \tag{5.8}$$

The influence of the nuclear spin in our further discussion then only appears in connection to the fundamental selection rule for bosons [27]:

$$N + I + S = even. \tag{5.9}$$

This rule severely limits the possible scattering states. In the doubly polarised ^{85}Rb-gas for example, I and S are odd so N can only be even!
In general, the orthogonal solutions of (5.3), when the last two terms are abandoned, are denoted by:

$$|^{2S+1}\Lambda_{\pi_e}(R) > \otimes\, |S\Sigma >, \tag{5.10}$$

where π_e denotes the electronic inversion symmertry (electronic parity) with respect to the midpoint of the line joining the nuclei. The eigenvalues of these adiabatic states (i.e. the singlet and triplet potential) are parametric functions of R. For large internuclear distances we may neglect overlap effects and a molecular state then asymptotically corresponds to two ground-state atoms A. Within the Heitler-London approximation [28], the singlet and triplet states are then given by linear combinations of products of atomic wavefunctions:

$$|^{2S+1}\Lambda_{\pi_e} > = \frac{1}{\sqrt{2}}\{|s>^1_A|s>^2_B + (-1)^S|s>^2_A|s>^1_B\}, \tag{5.11}$$

where we have suppressed the spin part and in addition, have only considered the valence electron states.
The electronic parity π_e is given by $(-1)^S$. In this notation $|s>^1_A$ means that electron 1 is in an s-state at nucleus A. Introducing the factor $(-1)^S$ assures that the states (5.11) are antisymmetric under electron interchange. In the special case of doubly-polarised atoms, the only possible molecular state is the $^3\Sigma_u$-triplet state, where we have used the usual spectroscopic notation Σ to express that $\Lambda = 0$. It is emphasised that the Heitler-London approximation (5.11) describes almost perfectly the ground-state channel in the photo-association process at the interatomic distances where this process takes place in

the experiments to be analysed.
For the moment this completes our discussion on the ground-states. In the next section we will discuss the interactions between the atoms in the excited molecule $A + A^*$.

5.3 Interactions between a ground-state and an excited atom.

The second ingredient necessary in the calculation of optical collisions is the set of excited-state ($A + A^*$) potentials and corresponding basis states. The Hamiltonian that describes a ground- and an excited state alkali atom at large distance is given by:

$$\hat{H} = \hat{T} + \hat{H}^{dd} + \sum_{k=1}^{2} \hat{H}_k^{so} + \sum_{k=1}^{2} \hat{H}_k^{hf}, \tag{5.12}$$

where $\hat{T}$ is the kinetic energy operator, $\hat{H}^{dd}$ is the electric dipole-dipole operator, $\hat{H}^{so}$ is the spin-orbit interaction and $\hat{H}^{hf}$ is the hyperfine interaction. The electric dipole-dipole interaction accounts for the resonant electric dipole interaction between the atoms. It is given by:

$$\hat{H}_{dd} = \frac{\vec{d}_1 \cdot \vec{d}_2 - 3(\vec{d}_1 \cdot \hat{R})(\vec{d}_2 \cdot \hat{R})}{4\pi\epsilon_0 R^3}, \tag{5.13}$$

in which $\vec{d}_1$ and $\vec{d}_2$ are the electric dipole-moment operators of atom 1 and 2, respectively, R is the internuclear distance and $\hat{R}$ the internuclear unit-vector. It is convenient in our further calculations to express $\hat{H}^{dd}$ in the molecular frame. Therefore we introduce the molecule-fixed spherical tensor operators

$$\begin{aligned} \hat{d}_{k\pm1} &= \mp\frac{\hat{d}_{k\xi} \pm i\hat{d}_{k\eta}}{\sqrt{2}}, \\ \hat{d}_{k0} &= \hat{d}_{k\zeta}, \end{aligned} \tag{5.14}$$

in which $\hat{d}_{k\xi}$ is the ξ^{th} component of the dipole operator of atom k. Equation (5.13) then transforms into:

$$\hat{H}_{dd} = -\frac{\hat{d}_{1+1}\hat{d}_{2-1} + \hat{d}_{1-1}\hat{d}_{2+1} + 2\hat{d}_{10}\hat{d}_{20}}{4\pi\epsilon_0 R^3}, \tag{5.15}$$

in which all operators are defined with respect to the molecular frame. From this expression it is also easily seen that $\hat{H}^{dd}$ conserves Λ: $\hat{d}_{1+1}$ increases, $\hat{d}_{2-1}$ decreases the respective atomic orbital angular momentum projections; furthermore, $\hat{d}_{k0}$ does not alter the projection of the orbital angular momentum of atom k so the net change in Λ is zero. Moreover the spin coordinates and the electronic inversion symmetry are not affected by $\hat{H}^{dd}$, so its eigenstates can be denoted by:

$$|^{2S+1}L\Lambda; \pi_e > \otimes |S\Sigma >. \tag{5.16}$$

The spin-orbit interaction describes the interaction between the orbital angular momentum $\vec{l}$ and the spin $\vec{s}$ *within* the excited atom: $\vec{l}$ and $\vec{s}$ couple to total electronic angular momentum $\vec{j}$. In an excited alkali atom A^*, $j = 1/2$ or $3/2$. The energy difference

between these atomic $P_{1/2}$ and $P_{3/2}$ levels is the fine-structure splitting ΔE. For the relatively large internuclear distances we are interested in, the interaction may be taken to be R-independent and can then effectively be represented by:

$$\hat{H}_k^{so} = \frac{2\ \Delta E}{3\hbar^2}\vec{l}_k \cdot \vec{s}_k, \tag{5.17}$$

in which $\vec{l}_k$ and $\vec{s}_k$ are the orbital and spin angular momentum of atom k (= effectively the orbital and spin angular momentum of the valence electron). Since $\hat{H}_{so}$ is invariant under simultaneous rotations of $\vec{l}$ and $\vec{s}$, the interaction is diagonal in the total electronic angular momentum quantum number j and its projection on an arbitrary axis. In the body-fixed frame $\hat{H}_{so}$ therefore transforms into:

$$\hat{H}_{so} = \sum_{j,m_j} \frac{a_{so}}{2}[j(j+1) - l(l+1) - s(s+1)]|(ls)jm_j;\zeta >< (ls)jm_j;\zeta| \tag{5.18}$$

The term $\hat{H}^{hf}$ represents the hyperfine interactions in the ground-state and in the excited state atom. The hyperfine interaction in the ground-state atom is the Fermicontact term, that was discussed in the preceding section. The hyperfine interaction in the excited atom is much weaker than the interaction in the ground-state atom [26]. Of all interactions in the Hamiltonian only the dipole interaction is R-dependent. If we imagine to slowly bring together the ground- and excited atom, then the dipole interaction will successively overwhelm all other interactions, starting with the hyperfine interaction in the excited atom. The distance where the dipole interaction becomes comparable to the hyperfine interaction in the excited atom is of the order of several thousands of a_0. The distance where the dipole interaction equals the hyperfine interaction in the ground-state atom is several hundreds of a_0. Therefore at the distances we are interested in, only the spin-orbit interaction needs to be taken into account and the influence of the hyperfine interaction can be neglected.

The adiabatic molecular potential curves for the $A + A^*$-molecule are then found by diagonalisation of the Hamilton-matrix H, defined by

$$H_{kl} =< \phi_k|\hat{H}_{dd} + \hat{H}_{so}|\phi_l >, \tag{5.19}$$

in which the set $\{|\phi_k >\}$ provides a repesentation for the molecular eigenstates. The R-dependent eigenvalues of this matrix are the required adiabatic molecular potentials. The term adiabatic is used in this context because we suppose the nuclei to move so slowly that their motion does not generate transitions between different adiabatic electronic states. Therefore the eigenvectors corresponding to the adiabatic potentials are the (adiabatic) molecular *eigenstates*. Since $(\hat{H}_{dd} + \hat{H}_{so})$ conserves the projection Ω of the total internal molecular angular momentum $\vec{J}$ and the electronic inversion symmetry π_e, we shall use the corresponding quantum numbers to label the adiabatic molecular states.

5.4 Basis states for alkali-dimer eigenstates.

In order to calculate the adiabatic Rb+Rb* potentials, we must choose a set of basis states for the Rb+Rb* molecule. With respect to this, it is convenient to have basis states that reflect the conservation laws (i.e. the symmetry properties) of the particular individual interactions. As we have seen in the previous section, at small inter-atomic distances the spin-orbit interaction is negligible compared to the dipole interacion. Because the electric dipole interaction conserves Λ, at these distances, the Hamiltonian will to a very good approximation be diagonal in Λ. It is therefore convenient to label the set of basiskets among others by the quantum number Λ, since the matrix representation of the Hamilton operator will then be approximately diagonal at small internuclear distances. The total projection of the molecular angular momentum on the internuclear axis (Ω) is rigorously conserved throughout the whole range of internuclear distances. Therefore in order to specify this quantum number, we need only add Σ in the notation, since Λ is already included. Finally, π_e is also conserved and therefore basiskets specifying L,Λ,S ,Σ and π_e provide a physically attractive set to specify the internal degrees of freedom of the molecule.

Put in formula, the above mentioned *normalised* kets are

$$|\phi> := |^{2S+1}L\Lambda, \pi_e> \otimes |S\Sigma>. \tag{5.20}$$

In this equation the part $|^{2S+1}L\Lambda, \pi_e>$ in the Heitler-London appoximation is given by:

$$|^{2S+1}\Lambda, \pi_e> = \frac{1}{2}\left[\{|s>^1_A|p_\Lambda>^2_B + (-1)^S|s>^2_A|p_\Lambda>^1_B\} - \pi_e\{|s>^1_B|p_\Lambda>^2_A + (-1)^S|s>^2_B|p_\Lambda>^1_A\}\right], \tag{5.21}$$

where we have used the same notation as in the case of two ground-state atoms. These states satisfy the required antisymmetry under exchange of electrons and have electronic parity π_e.

5.4.1 Reflection symmetry

In diagonalising the electronic Hamilton matrix (5.19) we will find it to be possible to assign an additional useful quantum number to the electronic eigenstates in cases that $\Omega = 0$, namely the reflection (anti)symmetry of the eigenstates relative to an *arbitrary* plane through the ζ-axis, for definiteness the $\xi - \zeta$-plane. Note that for $\Omega \neq 0$ it is not useful to introduce states with a definite reflection symmetry, since one needs definite superpositions of Ω and $-\Omega$ for another purpose, i.e. to form states of definite total parity.

Since we know beforehand that states with definite reflection symmetry will be eigenstates of the Hamilton matrix (5.19), we can profitably use this property in diagonalising the Hamiltonian matrix. To that end it is useful to point out that under reflection in the $\xi - \zeta$-plane, denoted by the operator $\hat{S}_{\xi\zeta}$, we have

$$\hat{S}_{\xi\zeta}\{\ |^{2S+1}L\Lambda, \pi_e > \otimes |S\Sigma >\ \} = (-1)^{\sum l_i}(-1)^{L-\Lambda}(-1)^{S-\Sigma}\ |^{2S+1}L - \Lambda, \pi_e > \otimes |S - \Sigma >, \tag{5.22}$$

where l_i denotes the atomic orbital angular momentum of atom i ($i = 1, 2$).
This follows from the fact that $\hat{S}_{\xi\zeta}$ can be written as the product $\hat{R}_{\pi\eta}\hat{P}$ of a rotation operator which rotates each electronic wavefunction over π about an axis *through its nucleus parallel to the η-axis* and an electronic inversion operation (parity operation) *with respect to its own nucleus.* Note that the s (p) state has even (odd) parity, which is accounted for by the factor $(-1)^{\sum l_i}$.
Furthermore, the transformations

$$|L\Lambda > \ \rightarrow\ (-1)^{L-\Lambda}|L - \Lambda > \tag{5.23}$$

$$|S\Sigma > \ \rightarrow\ (-1)^{S-\Sigma}|S - \Sigma >, \tag{5.24}$$

reflect the usual behaviour under the above-mentioned π-rotation. As a consequence we find the linear combinations

$$\frac{1}{\sqrt{2}}\{|^{2S+1}L\Lambda, \pi_e > \otimes |S\Sigma > \mp (-1)^{L-\Lambda}(-1)^{S-\Sigma}|^{2S+1}L - \Lambda, \pi_e > \otimes |S - \Sigma >\} \tag{5.25}$$

for $\Lambda > 0$ and $\Sigma = -\Lambda$ to have $\pm$ reflection symmetry.

The state $|^{2S+1}L\Lambda = 0, \pi_e > \otimes |S\Sigma = 0 >$ has reflection symmetry type $(-1)^{L+S+1}$ by itself.
Now that we have appropriate basiskets, we can calculate the matrixelements $H_{kl} =< \phi_k|\hat{H}_{dd} + \hat{H}_{so}|\phi_l >$ and the adiabatic $(A + A^*)$ potentials. This will be done in the next sections.

5.5 Adiabatic electric dipole-dipole potentials

Before turning to diagonalisation of the $(H_{dd} + H_{so})$-matrix, we shall first diagonalise the H_{dd} matrix. The resulting potentials will approximate the real molecular potentials rather accurately in the region where $\hat{H}_{dd}(R) >> \hat{H}_{so}$. This region is particularly large for light elements (e.g. Li), since the spin-orbit interaction because the fine-structure splitting ΔE is very small in those atoms. In the limit of small internuclear distances the adiabatic molecular potentials of *any* alkali dimer asymptotically coalesce with the electric dipole potentials V_{dd} because $V_{so} << V_{dd}$ is then always satisfied.
The matrix $V_{kl}^{dd}(R) =< \phi_k|\hat{H}_{dd}|\phi_l >$, is diagonal in Λ:

$$\begin{aligned} \Lambda &= \pm 1 : V_{dd}(R) = \frac{(-1)^{S+1}\pi_e d^2}{4\pi_e \epsilon_0 R^3}\delta_{SS'}\delta_{\Sigma\Sigma'}\delta_{\pi_e\pi'_e}, \\ \Lambda &= 0 : V_{dd}(R) = \frac{2(-1)^{S}\pi_e d^2}{4\pi_e \epsilon_0 R^3}\delta_{SS'}\delta_{\Sigma\Sigma'}\delta_{\pi_e\pi'_e}, \end{aligned} \tag{5.26}$$

where d is the atomic dipole matrix element, $d =< l' = 1\ m'_l = 0|d_\zeta|l = 0\ m_l = 0 >$, in which the quantum numbers used in the bra and the ket are the orbital atomic angular momentum of the valence electron and its projection on the internuclear axis. The resulting potentials, furnished with their Hund's case (a) labels $^{2S+1}|\Lambda|^{\pm}_{g/u}$ are shown below.

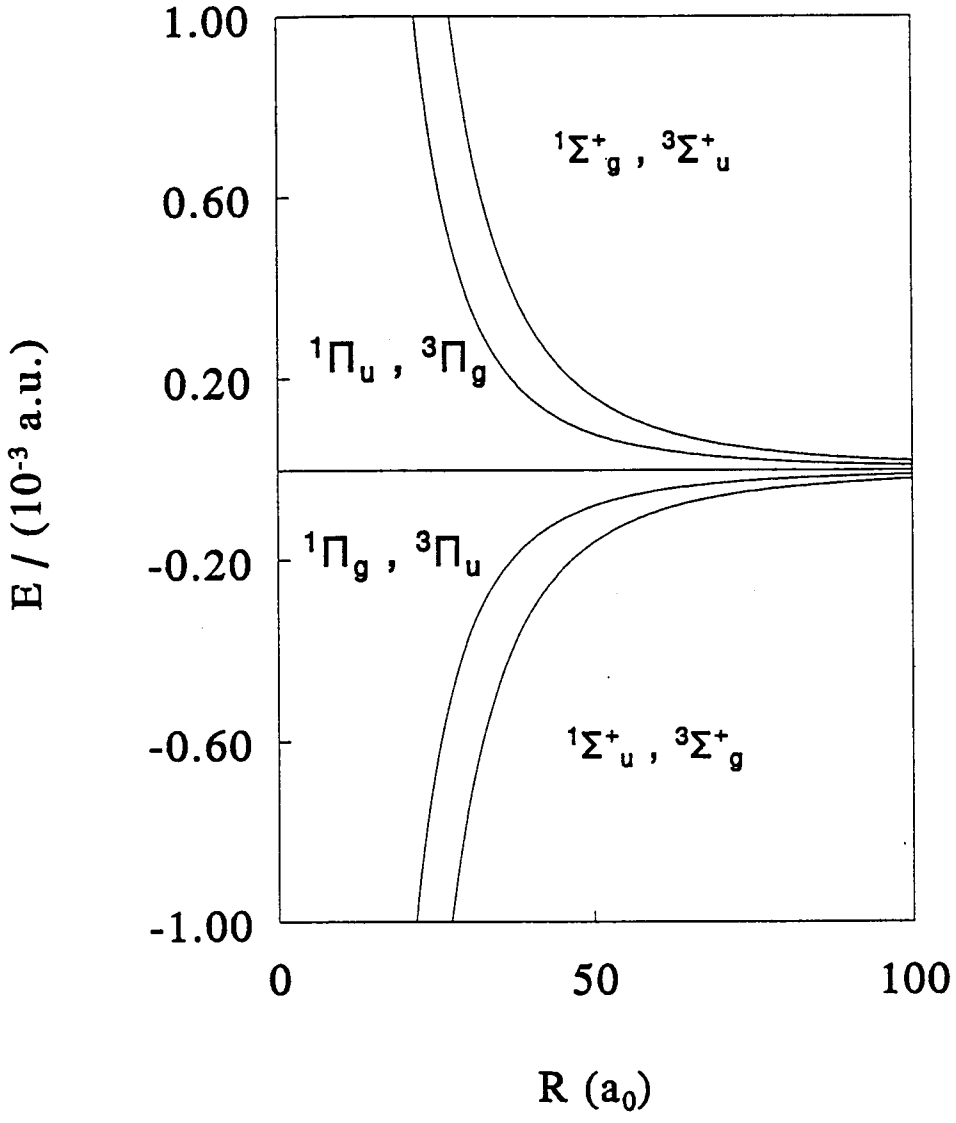

Figure 5.1: (Rb+Rb*) adiabatic electric dipole-dipole potentials

5.6 Adiabatic potentials including spin-orbit interaction

As we have seen in the section 5.3, both $\hat{H}_{dd}$ and $\hat{H}_{so}$ conserve Ω. Therefore the total Hamilton matrix defined by $H_{kl} = < \phi_k | \hat{H}_{dd} + \hat{H}_{so} | \phi_l >$ consists of three submatrices, corresponding to molecular states with the quantum numbers $\Omega = 0, 1$ and 2.
Those with $\Omega = -1$ and -2 are identical to the $\Omega = 1, 2$ matrices.

In order to illustrate the calculation of some adiabatic potentials, we confine our attention to the $\Omega = 0$ states. In abbreviated notation, we have the two basis states

$$\begin{aligned} \phi_1^+(\Omega = 0) &= |\Lambda = 0, S = 0, \Sigma = 0, \pi_e >, \\ \phi_2^+(\Omega = 0) &= \frac{1}{\sqrt{2}} \{ \, |\Lambda = 1, S = 1, \Sigma = -1, \pi_e > - |\Lambda = -1, S = 1, \Sigma = 1, \pi_e > \, \} \end{aligned} \tag{5.27}$$

for + reflection symmetry (0^+ subspace) and

$$\begin{aligned} \phi_1^-(\Omega = 0) &= |\Lambda = 0, S = 1, \Sigma = 0, \pi_e >, \\ \phi_2^-(\Omega = 0) &= \frac{1}{\sqrt{2}} \{ \, |\Lambda = 1, S = 1, \Sigma = -1, \pi_e > + |\Lambda = -1, S = 1, \Sigma = 1, \pi_e > \, \} \end{aligned} \tag{5.28}$$

for $-$ reflection symmetry (0^- subspace). Therefore, in order to calculate the adiabatic $\Omega = 0$-potentials, we must diagonalise simple 2×2 matices. Upon calculation these turn out to be

$$0^+ : \begin{bmatrix} \frac{2\pi_e d^2}{4\pi\epsilon_0 R^3} & -\frac{\sqrt{2}}{3}\Delta E \\ -\frac{\sqrt{2}}{3}\Delta E & \frac{\pi_e d^2}{4\pi\epsilon_0 R^3} - \frac{\Delta E}{3} \end{bmatrix}, \tag{5.29}$$

$$0^- : \begin{bmatrix} \frac{-2\pi_e d^2}{4\pi\epsilon_0 R^3} & \frac{\sqrt{2}}{3}\Delta E \\ \frac{\sqrt{2}}{3}\Delta E & \frac{\pi_e d^2}{4\pi\epsilon_0 R^3} - \frac{\Delta E}{3} \end{bmatrix}. \tag{5.30}$$

In a similar way, $\Omega = 1$ states originate from the basis states

$$\begin{aligned} \phi_1(\Omega = 1) &= |\Lambda = 0, S = 1, \Sigma = 1 >, \\ \phi_2(\Omega = 1) &= |\Lambda = 1, S = 1, \Sigma = 0 >, \\ \phi_3(\Omega = 1) &= |\Lambda = 1, S = 0, \Sigma = 0 > \end{aligned} \tag{5.31}$$

and the corresponding matrix can be calculated analogously.

The adiabatic potentials are found upon solving the characteristic equations of the associated matrices. The resulting potentials are shown below.

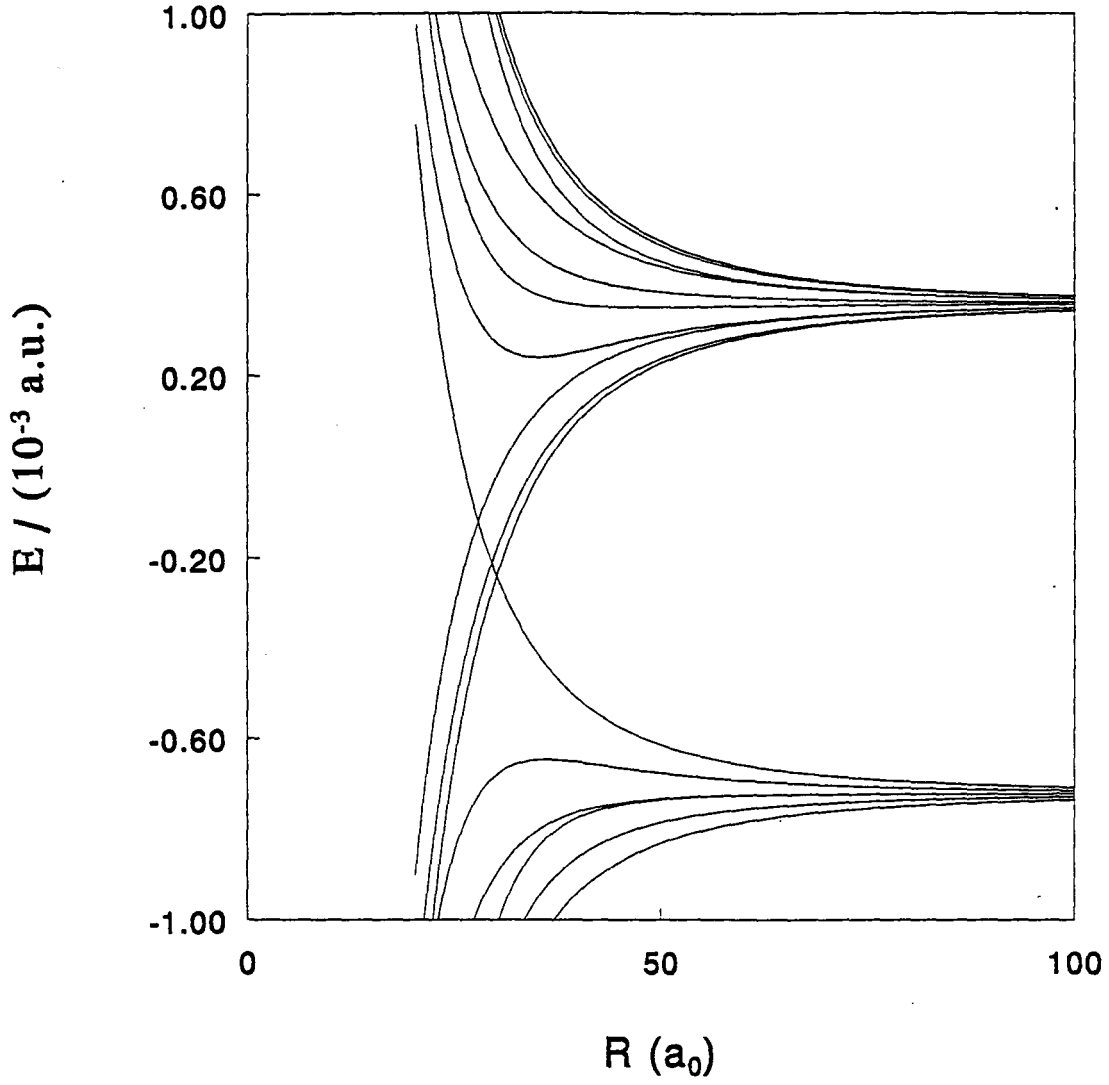

Figure 5.2: (Rb+Rb*) adiabatic potentials. The appropriate labels of the potentials are given in fig 5.3.

In connection with the calculations above it is convenient to introduce new variables

$$Y := \frac{V - E_{1/2}}{\Delta E},$$
$$X := \frac{d^2}{12\pi\epsilon_0 R^3 \Delta E}. \tag{5.32}$$

This means that the adiabatic potentials (V) are defined relative to the energy of the asymptotic atomic $P_{1/2}$ level (which has energy $E_{1/2}$), expressed in terms of the fine-structure splitting ΔE. The characteristic equations then become:

$$0^+_{\pi_e} \; : \; Y^2 - (1 + 9\pi_e X)Y + (4\pi_e X + 18X^2) = 0 \tag{5.33}$$
$$0^-_{\pi_e} \; : \; Y^2 - (1 - 3\pi_e X)Y - 18X^2 = 0 \tag{5.34}$$
$$1_{\pi_e} \; : \; Y^3 + (6\pi_e X - 2)Y^2 + (1 - 8\pi_e X - 9X^2)Y + (2\pi_e X + 6X^2 - 54\pi_E X^3) = 0 \tag{5.35}$$
$$2_{\pi_e} \; : \; Y = 1 + 3\pi_e X \tag{5.36}$$

The corresponding solutions are presented below.

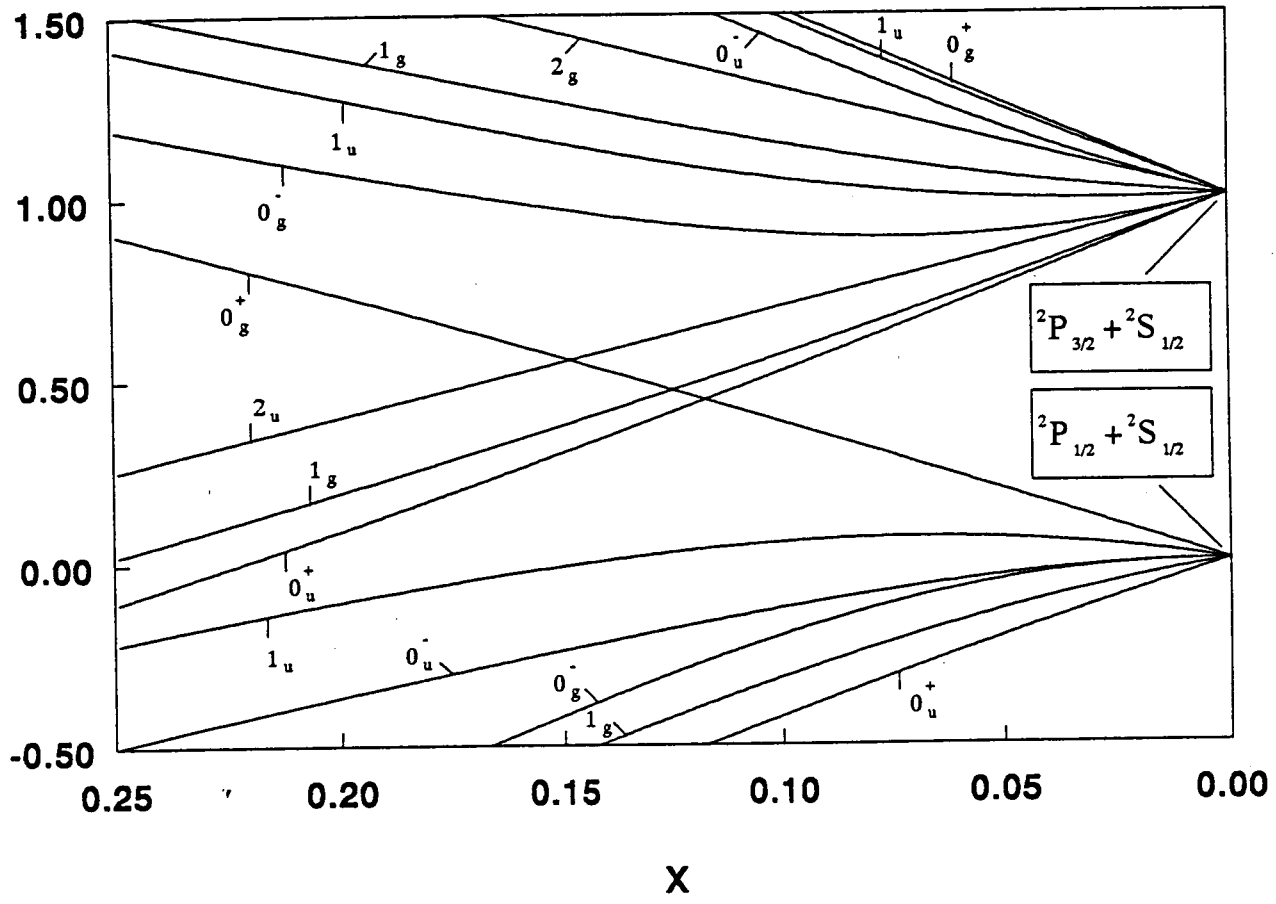

Figure 5.3: (Rb+Rb*) adiabatic potentials, scaled using X and Y

As mentioned in the preceding section, the adiabatic potentials approach the four electric dipole potentials for small internuclear distances, where the R-independent spin-orbit interaction becomes negligible compared to the $1/R^3$ dipole interaction. In this region the potentials are commonly denoted by the Hund-case (a) labels ${}^{(2S+1)}\Lambda_{\pi_e}$.

In the limit $R \rightarrow \infty$, the electric dipole interaction vanishes and the "molecule" dissociates into a ground-state and an excited atom. At these large distances the energy relative to the $S_{1/2} - S_{1/2}$ ground-state asymptote stems entirely from the excited atom.
Thus for $R \rightarrow \infty$ *all* adiabatic molecular potentials correlate either to the $S_{1/2} - P_{1/2}$ or the $S_{1/2} - P_{3/2}$ state, differing in energy by the amount of the atomic fine-structure splitting ΔE, as can be seen from fig 5.3 for $X \rightarrow 0$.

In the construction of the set for the molecular states we made heavily use of *internally* conserved observables, neglecting molecular rotation. But the molecules are allowed to rotate and associated with this motion is the relative molecular orbital angular momentum N. It is therefore natural, in order to squeeze as many commuting observables as possible from a given molecular state, to extend the kets with P and M_P as has already been discussed in chapter 4.
Then the general conservation of the total angular momentum $\vec{P}$, ($\vec{P} = \vec{J} + \vec{N}$), and its projection M_P on the space-fixed z-axis can be applied to the molecule.

Put in formula, the above mentioned *normalised* "generalised" kets become

$$|\phi> := |^{2S+1}L\Lambda, \pi_e> \otimes |S\Sigma> \cdot \sqrt{\frac{2P+1}{8\pi^2}} D^{P*}_{M_P\Omega}(\alpha, \beta, \gamma). \tag{5.37}$$

These kets will be used in the next section, where we will derive the coupled channels equations resulting from non-adiabaticity due to molecular motion.
Furthermore they play an important role in section 6.2 in the calculation of the angular dependent part of the transition matrix element associated with the photo-association.

5.7 Coupled channels equations

As was already mentioned in the preceding section, the nuclear motion generates coupling between different adiabatic states, i.e. the local Hund's case c *electronic* eigenstates found in section 5.6, supplemented by the P, Ω and M_P dependent *rotational* part. To derive the equations that describe this coupling, we start from the Schrödinger equation for the two atom system:

$$\hat{H}\Psi(\vec{R},\vec{r}) = E\Psi(\vec{R},\vec{r}), \tag{5.38}$$

where E is the total energy of the two-atom system and

$$\hat{H} = -\frac{\hbar^2}{2\mu}\nabla^2_{\vec{R}} + E_k(R). \tag{5.39}$$

Here $E_k(R)$ is the adiabatic electronic eigenvalue with R-dependent adiabatic electronic eigenfunctions $|\kappa\Omega;\zeta,R;PM_P>$, κ summarizing any other quantum numbers needed to specify the electronic state uniquely. For the sake of simplicity we have denoted $|\kappa\Omega;\zeta,R;PM_P>$ by $|k>$, where k specifies the set of quantumnumbers κ,Ω P and M_P.

The first term in (5.39) represents the kinetic energy operator for the motion of the nuclei. This motion can be separated into radial and angular motion:

$$-\frac{\hbar^2}{2\mu}\nabla^2_{\vec{R}} = -\frac{\hbar^2}{2\mu R}[\frac{\partial^2}{\partial R^2}R] + \frac{\hat{\vec{N}}^2}{2\mu R^2}. \tag{5.40}$$

The first term stems from the radial motion of the nuclei. It induces coupling between the different *adiabatic electronic eigenstates*, because these *eigenstates* are R-dependent linear combinations of the states $|L\Lambda S\Sigma PM_P>$; if we denote an adiabatic eigenstate by $|\kappa\Omega;\zeta,R;PM_P>$, where κ and Ω are the quantum numbers to specify the adiabatic eigenstate uniquely then:

$$|\kappa\Omega;\zeta,R;PM_P> = \sum_{L\Lambda S\Sigma} g^{\kappa}_{L\Lambda S\Sigma}(R)|L\Lambda S\Sigma PM_P> . \tag{5.41}$$

The second term in (5.39) represents the rotational motion of the nuclei. It induces coupling between adiabatic eigenstates differing in Ω.
This can be seen using the identity $\vec{N} = \vec{P} - \vec{J}$; substituting this in the second term of (5.39) yields

$$\frac{\hat{\vec{N}}^2}{2\mu R^2} = \frac{1}{2\mu R^2}[\hat{\vec{P}}^2 - \hat{P}^2_\zeta + \hat{\vec{J}}^2 - \hat{J}^2_\zeta - \hat{P}_+\hat{J}_- - \hat{P}_-\hat{J}_+]. \tag{5.42}$$

Obviously the first four terms in (5.42) are diagonal in P, M_P, J and Ω. The last two terms, however, consist of ladder operators that generate coupling between adiabatic eigenstates that differ in Ω by one. Remember that $\hat{P}_+$ *decreases* Ω and $\hat{P}_-$ *increases* Ω by one since these operators are defined with respect to the molecular frame here.

If we now set

$$|\Psi(R,\vec{r})>=\sum_k \frac{F_k(R)}{R}|k>, \tag{5.43}$$

substitution in the Schrödinger equation leads to the coupled equations:

$$F_k''(R)+[\frac{2\mu}{\hbar^2}(E-E_k(R)-P(P+1)+\Omega^2]F_k(R)= \tag{5.44}$$

$$\sum_i[-2F_i'(R)<k|\frac{\partial}{\partial R}|i>+F_i(R)(\frac{<k|\hat{\vec{J}}^2-\hat{J}_\zeta^2|i>}{R^2}-\frac{<k|\hat{P}_+\hat{J}_-+\hat{J}_-\hat{P}_+|i>}{R^2}-<k|\frac{\partial^2}{\partial R^2}|i>)].$$

Depending on the particular dependence of the states $|i>$ on R, some terms in (5.44) may be neglected, e.g. if $|i>$ is a slowly varying function of R, then the terms $<k|\frac{\partial}{\partial R}|i>$ and $<k|\frac{\partial^2}{\partial R^2}|i>$ can be omitted. This latter approximation is in fact introduced for the relevant large distances in the actual calculations. In the next section we will consider the importance of the rotational coupling between the excited states.

5.8 Rotational coupling

In this section we will discuss the non-adiabatic rotational coupling terms in (5.44), that induce transitions between *adiabatic* eigenstates. This coupling reflects the fact that instead of the molecule (space) fixed coordinate system in which the wavefunction is specified, the space (molecule) fixed system becomes physically more appropriate as a reference system: at large distances, the interaction between the atoms is weak and $\vec{J}$ and $\vec{N}$ are more or less independently conserved so the space fixed z-axis is most appropriate as axis of quantisation. When the atoms approach each other, however, the coupling between $\vec{J}$ and $\vec{N}$ becomes more prominent and $\vec{J}$ becomes locked to the internuclear axis, following the rotation of the internuclear axis, leading to the *adiabatic* eigenstates of section (5.6). In case the adiabatic eigenstates are selected as basis states, it will be neccesary in general to include the coupling between these induced by the finite rotational angular velocity. This is called the *rotational* coupling, which should be viewed as a second type of non-adiabatic coupling in addiation to the *radial* coupling induced by the $\partial/\partial R$ and the $\partial^2/\partial R^2$ non-adiabatic coupling terms in (5.44). It is due to the fact that the rotation of the molecule fixed frame can be so rapid that the total electronic angular momentum $\vec{J}$ can no longer follow this motion. Alternatively this can be visualised as if the molecule-fixed frame slips away under the electonic angular momentum $\vec{J}$. Consequently, the projection of $\vec{J}$ on the internuclear axis will change, thus implying a transition to another *adiabatic* eigenstate characterised by Ω', with $\Omega' = \Omega \pm 1$.

From an energetic point of view, the relative importance of these non-adiabatic transitions depends on the magnitude of the rotational energy $E_{rot}(R)$ compared to the energy-splitting of the adiabatic potentials, $\Delta E_{\Omega\Omega'}(R) = E_{\Omega}(R) - E_{\Omega'}(R)$.
When $E_{rot} << \Delta E_{\Omega\Omega'}$, $\vec{J}$ can be considered anchored to the internuclear axis and Ω is conserved. If, on the other hand, $E_{rot} >> \Delta E_{\Omega\Omega'}$, non-adiabatic coupling becomes very important. The latter is anyhow the situation for large internuclear distances.
Often the so-called *locking-radius*, R_L, defined by the relation [24]

$$\Delta E_{\Omega\Omega'}(R_L) = \frac{\hbar^2 N(N+1)}{2\mu R_L^2}, \tag{5.45}$$

is used as a measure for the distance at which the adiabatic description breaks down, i.e. the distance where $\vec{J}$ is no longer "locked" (anchored) to the internuclear axis.
In order to determine the importance of the rotational coupling terms in the case of ^{85}Rb, we have compared the energy difference between the 0_g^- and the 1_g $(S_{1/2} - P_{1/2})$ potentials with some typical rotational energies over the relevant range of internuclear distances 5 to 80 a_0.
To that end, we have first constructed model potentials for the 0_g^- and 1_g excited states. For the short-range part 8 to 20 a_0 of the potentials we have used the potentials given by Spiegelmann [29]. These potentials, however, do not include spin-orbit coupling. Therefore, in order to include this interaction in the *adiabatic* eigenpotentials, we have added an R-independent non-diagonal coupling term in the Hamiltonian and subsequently diagonalised

the resulting Hamilton matrices, according to the procedure that was outlined in section (5.6). The resulting potentials were then connected differentiably to their long-range tails.

Fig 5.4 shows the resulting energy difference between the 0_g^- and 1_g curves as well as the rotational energies for two typical N-values.

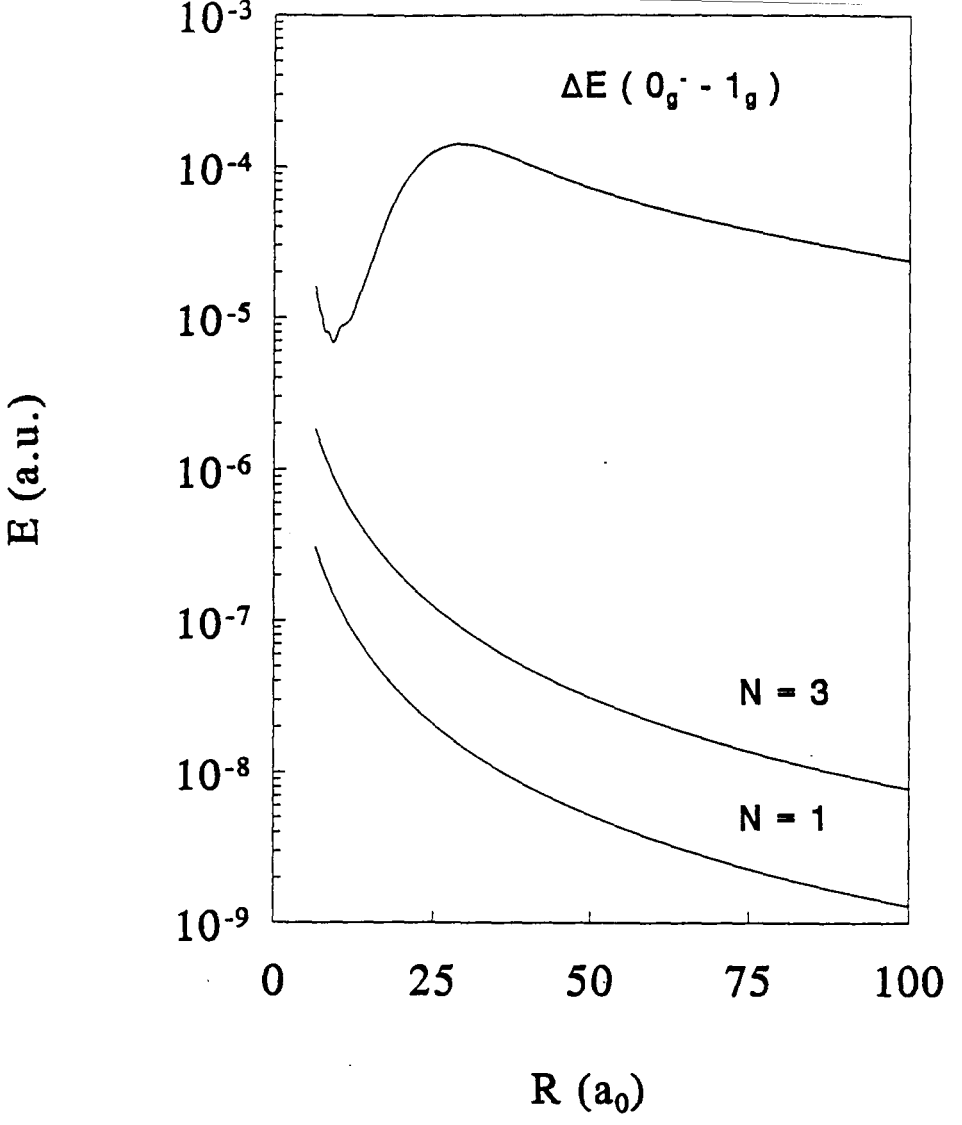

Figure 5.4: Energy splitting between the 0_g^- and 1_g ($S_{1/2}$-$P_{1/2}$) curves and rotational energies for $N = 1$ and $N = 3$

As can be seen from this figure, in our case of ^{85}Rb, the rotational energy is very small compared to the energy splitting of the 0_g^- and 1_g curves *over the whole range of relevant internuclear distances.* Note that the range of very large distances where the rotational coupling is important (i.e. outside the locking-radius), is not relevant for the photo-association calculations. Moreover we point out that the energy splitting between the 0_u^+ and the 1_u ($S_{1/2} - P_{1/2}$) states, as well as that between the states that differ in Ω by 1 that asymptotically connect to the $S_{1/2} - P_{3/2}$ level, is even larger than the above depicted splitting of the 0_g^- and 1_g curves.
This means that we do not need to take rotational coupling into account in our calculations.

Chapter 6

Laser-coupling

In this chapter we discuss the transition, induced by laser radiation, from the two-particle continuum ground-state $(A + A)$ to a bound "molecular" state in the excited $(A + A^*)$ potential, i.e. photo-association. Since the initial state is a *continuum* ground-state it is not at all clear beforehand, how to take care of the normalisation of the ground-state wavefunction. Furthermore, we must derive the distribution (coherent or incoherent?) of the relative atomic orbital angular momenta (N) in the ground-state, since this distribution determines the form of the photo-association spectrum.
In order not to tackle all problems at once, we divide the problem into two subproblems: we first concentrate on the "normalisation" and the relative distribution of the relative atomic orbital angular momenta in the ground-state, using a simple two-channel model for the photo-association process. Once this problem is solved, in section 6.2 we shall leave the assumption of a spherically symmetric coupling potential, and we introduce the angular dependence of the coupling. To that end we shall consider the angular dependence of both the wavefunctions and the (angular dependent) laser-coupling. This angular dependent part of the transition matrix element entails the important selection rules that govern the photo-association.
Combining the distribution of the relative atomic orbital angular momenta in the ground-state and the angular part of the transition matrix element, which incorporates the important selection rules, we have at our disposal the instruments nessecary to calculate the (theoretical) photo-association spectrum!

6.1 Normalisation of the ground-state wavefuntion and the distribution of the relative orbital angular momenta in the ground-state

Our final goal is to derive an expression for the transition probability per unit time from the initial two-particle *continuum* ground-state wavefunction (A+A) to a *bound* state in the excited $(A + A^*)$ potential. A complication arises with respect to this because the initial ground-state is in the continuum energy spectrum and consequently can not be normalised in the usual sense. Therefore one cannot use Fermi's Golden Rule directly. As was already pointed out above, we must also find the distribution of the relative atomic orbital angular momenta in the ground-state.

In order to discuss these matters, let us start from a simple two-channel model. The ground-state potential $V_g(R)$ is taken to be zero, so the initial motion corresponds to the free motion of a two-particle "wave-packet". This simplification will prove quite practical: it is physically acceptable since indeed for large internuclear distances the atomic interaction vanishes so the motion asymptotically corresponds to free motion. Moreover this model incorporates all features that arise in connection with the actual photo-association i.e., the "normalisation" of the continuum states and the distribution over the relative atomic orbital angular momentum eigenstates.

The potential of the excited state is denoted by $V_e(R)$. The coupling between the two channels due to a laser of frequency ω_L, is denoted by V_c.

In our case $V_c = -\vec{d} \cdot \vec{E}_L$, where $\vec{d} = \vec{d}_1 + \vec{d}_2$, the sum of the atomic electric dipole moments and $\vec{E}_L$ is the electric field of the laser. As was already mentioned, in this section we want to focus on the problems associated with the ground-state so we take V_c to be a spherically symmetric potential, independent of the internuclear distance R; the angular dependence of V_c will be the subject of the next section. The wave-functions ψ will be taken to have the form $\psi = \phi\chi$, where ϕ denotes the "external" orbital motion of the two-particle wave-packet and χ specifies the internal and angular degrees of freedom of the "molecular" system.

In the ground-state e.g. $\phi \sim e^{i\vec{k}\vec{R}}$ and $\chi = |JM_J>$. Once the decomposition of ϕ in states of well-defined relative orbital angular momenta (i.e. the partial wave decomposition) is known, we can combine this information with the kets $|JM_J>$ to form the "generalised" kets $|J\Omega PM_P>$ that were introduced in chapter 4.

In order to get a firmer grasp on the physical meaning of ϕ, let us consider the atoms in the gas.

At large distances the interaction between two colliding atoms is negligible, so ϕ is proportional to the plane wave $e^{i\vec{k}\vec{R}}$. If we assume that the gas is distributed homogeneously and in thermal equilibrium in all directions, then the wave-vectors $\vec{k}$ are distributed isotropically in $\vec{k}$-space since there is no preferred direction in space for the atoms to align their collision trajectory. The resulting (ensemble) distribution of the wave-packets in $\vec{k}$-space shall be denoted by $\tilde{P}(\vec{k})$. This distribution can be decomposed into a part $f(k)$ that is

only dependent on the magnitude k, $k = |\vec{k}|$ and a part $g(\hat{k})$, where $\hat{k} = \vec{k}/k$, that describes the angular distribution of $\vec{k}$. Thus

$$\tilde{P}(\vec{k}) = f(k) \cdot g(\hat{k}). \tag{6.1}$$

By assumption $\vec{k}$ is distributed isotropically, so $g(\hat{k})$ reduces to a constant function. The distribution of k, $f(k)$, of course depends on the temperature of the gas and is generally taken to correspond to the Maxwell-Boltzmann distribution.

The transition probability per unit time for a transition from a continuum ground-state with energy E_g to the bound state with energy E_e in the excited potential, denoted by $P_{g\to e}$, is obtained by generalising the famous Fermi's Golden Rule

$$P_{g\to e} = \frac{2\pi}{\hbar}\int_0^\infty dE \int d\hat{k}| < \psi_e|V_c|\psi_g(E,\hat{k}) > |^2 P(E,\hat{k})\delta(E_e - E_g - \hbar\omega_L). \tag{6.2}$$

In this expression we have replaced $\tilde{P}(\vec{k})$ by its equivalent (Maxwell-Boltzmann) energy distribution $P(E,\hat{k})$, which is the probability to find in the ground-state a collision energy E and a "collision trajectory" in the $\hat{k}$ direction.
The ground-state functions $\psi_g(E,\hat{k})$, proportional to the plane waves $e^{i\vec{k}\vec{R}}$, are supposed to be energy and direction normalised:

$$< \psi_g(E,\hat{k})|\psi_g(E',\hat{k}') >= \delta(E - E')\delta(\hat{k} - \hat{k}'). \tag{6.3}$$

Note that the δ-function in (6.2) guarantees conservation of energy during the photo-association transition.

Furthermore, from (6.2), we readily obtain the relative distribution of the relative atomic orbital angular momenta N. To that end, we replace the plane wave travelling in the direction $\hat{k}$ by its *partial wave decomposition*

$$e^{i\vec{k}\vec{R}} = 4\pi \sum_{N=0}^{\infty}\sum_{M_N=-N}^{N} i^N j_N(kR) Y_{NM_N}(\hat{R}) Y^*_{NM_N}(\hat{k}). \tag{6.4}$$

Here, Y_{NM_N} is the well-known spherical harmonic and $j_N(kR)$ denotes the spherical Besselfuction.

Substitution of (6.4) in (6.2) and integrating over $\hat{k}$, learns that coherent contributions (interference of partial waves differing in N) cancel out, so eventually only incoherent terms remain in (6.2). Therefore, the *relative* contribution of the partial waves in (6.2) is in particular determined by the factor $(2N + 1)$, as can be verified from (6.4)

So, we have solved the first part of the photo-association calculation in that we were led to the incoherence of the ground-state partial wave contributions to the photo-association rates as well as their relative abundance. Clearly, detailed knowledge of this distribution is of crucial importance since the form of the theoretical photo-association spectrum (i.e. the relative height of the peaks) is very sensitive to fluctuations in the partial wave distribution. Note that the method outlined above is easily generalised to more complex situations in which $V_g(R)$ is a non-trivial function of R.

6.2 Laser-coupling: angular dependence

In order to calculate the relative "production rate" of the excited states out of ground-states, we must know both the relative contribution of the relative atomic orbital angular momenta in the ground-state and the matrix elements associated with these transitions. Since the distribution of the relative atomic orbital angular momenta in the ground-state has been determined in the previous section, we are left to calculate the matrix elements $< \psi_e|\vec{d}\cdot\vec{E}_L|\psi_g(E,\hat{k}) >$.

As was already pointed out in the previous section, the molecular states $\psi_g(E,\hat{k})$ and ψ_e can be separated into two parts: the one part (ϕ) describes the external motion of the wave-packet and is R-dependent, the other part (χ) contains information about the angular and internal degrees of freedom. The calculation of the matrix-element above therefore essentially reduces to an integral over the radial motion, times a matrix-element that contains the internal and angular dependence. The integral over R depends on the particular form of the potentials $V_g(R)$ and $V_e(R)$ and in practice can only be evaluated numerically. The angular part, however, can be evaluated exactly , as will be shown below, and it is this part that entails the important selection rules.
We shall take the radial integral for granted and concentrate on the internal and angular part of the above-mentioned matrix element. To that end we combine the internal part (χ) with the rotational part $|NM_N;z>$ to form "generalised" kets (see chapter 4), i.e. we concentrate on

$$< \Omega^{\pm}_{\pi_e}, \tilde{P}\tilde{M}_P|\vec{d}\cdot\vec{E}_L|SM_SNM_N;z> . \tag{6.5}$$

The explicit appearence of the relative orbital angular momentum N in the ket, once more, stresses the important role of the distribution of N in theoretical calculations.

Here, the ground-states are defined with respect to the space-fixed system because in the case of doubly-polarised atoms, which we are particularly interested in, the orientation of the atomic spins is known with respect to a space-fixed axis. These states can be linearly combined to form states of well-defined total angular momentum P:

$$.|SM_SNM_N;z> = \sum_{PM_P} < SM_SNM_N|PM_P >|(SN)PM_P;z>. \tag{6.6}$$

In order to calculate the matrixelements above, we express $|(SN)PM_P;z>$ in the body-fixed states, using equation (4.15):

$$|(SN)PM_P;z> = \sum_{\Omega}(-1)^{S-\Omega}< S-\Omega P\Omega|N0 > |S\Omega PM_P >. \tag{6.7}$$

In order to calculate the matrix-element in the molecular frame, the components of the electric field of the laser, $\vec{E}_L$, must be determined in that frame. This is most easily done if we express them in spherical components:

$$\begin{aligned} E_{\pm 1} &= \mp \frac{E_x \pm i E_y}{\sqrt{2}} \\ E_0 &= E_z. \end{aligned} \tag{6.8}$$

The spherical components E'_q of $\vec{E}_L$ with respect to the molecular frame are related to those in the space-fixed system, E_n, by the transformation

$$E'_q = \sum_n D^1_{nq}(\alpha, \beta, \gamma) E_n. \tag{6.9}$$

Furthermore,

$$\vec{d} \cdot \vec{E}_L = \sum_{q=-1}^{1} (-1)^q d'_q E'_{-q} = \sum_{n=-1}^{1} \sum_{q=-1}^{1} (-1)^q d'_q E_n D^1_{n\ -q}(\alpha, \beta, \gamma). \tag{6.10}$$

The state $|\Omega^{\pm}_{\pi_e} \tilde{P} \tilde{M}_P >$ consists of linear combinations of the states

$$\begin{aligned} |\tilde{L}|\tilde{\Lambda}|\tilde{S}\tilde{\Sigma}\tilde{P}\tilde{M}_P > = \frac{1}{2} \frac{1}{\sqrt{2(1+\delta_{\tilde{\Lambda}0}\delta_{\tilde{\Sigma}0})}} \sqrt{\frac{2\tilde{P}+1}{8\pi^2}} [|\tilde{L}\tilde{\Lambda}\tilde{S}\tilde{\Sigma}> D^{\tilde{P}*}_{\tilde{M}_P \tilde{\Omega}}(\alpha, \beta, \gamma) + \\ + (-1)^{P+L+S} |\tilde{L}\tilde{-\Lambda}\tilde{S}\tilde{-\Sigma}> D^{\tilde{P}*}_{\tilde{M}_P\ \tilde{-\Omega}}(\alpha, \beta, \gamma)]. \end{aligned} \tag{6.11}$$

Calculation of $< \Omega^{\pm}_{\pi_e} \tilde{P} \tilde{M}_P | \vec{d} \cdot \vec{E}_L | S M_S N M_N; z >$ therefore typically reduces to calculation of terms like:

$$\kappa := < \tilde{L}\tilde{\Lambda}\tilde{S}\tilde{\Sigma}\tilde{P}\tilde{M}_P | \vec{d} \cdot \vec{E}_L | S M_S N M_N; z >. \tag{6.12}$$

Upon using (6.6) and (6.7) we get

$$\kappa = \sum_{P,M_P} \sum_{\Omega} (-1)^{S-\Omega} < SM_S NM_N | PM_P > < S - \Omega P \Omega | N0 > < \tilde{L}\tilde{\Lambda}\tilde{S}\tilde{\Sigma}\tilde{P}\tilde{M}_P | \vec{d}\cdot\vec{E}_L | 00 S\Omega P M_P >. \tag{6.13}$$

The electric dipole operator only affects the orbital degrees of freedom, so the matrixelement (6.12) is diagonal in the electronic spin. After substitution of (6.10) and (6.11) into (6.13) and integrating over α, β and γ, we finally obtain (see appendix):

$$\kappa = \frac{1}{2} \frac{1}{\sqrt{2(1+\delta_{\tilde{\Lambda}0}\delta_{\tilde{\Sigma}0})}} \sqrt{(2\tilde{P}+1)}\delta_{S\tilde{S}}$$

$$\sum_n \sum_q \sum_{P,M_P} \sum_{\Omega} \sqrt{2P+1}(-1)^q < SM_S NM_N | PM_P > < S - \Omega P \Omega | N0 >$$

$$\left[\delta_{\tilde{\Sigma}\Omega} < 1\tilde{\Lambda} | d'_q | 00 > (-1)^{S+M_P} \begin{pmatrix} \tilde{P} & 1 & P \\ \tilde{M}_P & n & -M_P \end{pmatrix} \begin{pmatrix} \tilde{P} & 1 & P \\ \tilde{\Omega} & -q & -\Omega \end{pmatrix} E_n \right] +$$

$$(-1)^{\tilde{P}+M_P+1} \left[\delta_{-\tilde{\Sigma}\Omega} < 1 - \tilde{\Lambda} | d'_q | 00 > \begin{pmatrix} \tilde{P} & 1 & P \\ \tilde{M}_P & n & -M_P \end{pmatrix} \begin{pmatrix} \tilde{P} & 1 & P \\ -\tilde{\Omega} & -q & -\Omega \end{pmatrix} E_n \right]. \tag{6.14}$$

This is a very important formula since it allows us to calculate the angular part of the transition matrix elements *exactly*! It is of great importance in the calculation of theoretical spectra since it entails the important selection rules that govern the photo-association, embodied e.g. in the three-j-symbols. Apart from determining the relative peak heights in the photo-association spectra, equation (6.14) reflects conservation of *total* (= molecular + photon) angular momentum: when the initial state, which has total angular momentum P, absorbs a photon, then the final state can only have total angular momentum $\tilde{P}$ equal to P-1, P or P+1, as is guaranteed by the upper rows in the three-j-symbols. Similarly, the second rows express conservation of the *projection* of the total angular momentum, both in the space-fixed and in the molecular coordinate frame.

Since this graduation work, this formula has already succesfully been applied in the description of experimental photo-association specta.

Chapter 7

Conclusions

From this graduation report we may extract the following results:

- The photo-association process has been studied. Photo-association experiments provide a very elegant way to perform very high resolution spectroscopy on ultra-cold atoms. The spectroscopic data can be used to derive the interaction potential of colliding atoms.
  In this report, we have worked out the model to theoretically calculate such spectra, in particular:

- The excited-state potentials of alkali atoms have been calculated in the long-range part where the photo-association process takes place. The symmetry properties of these states have been determined since these play an important role in the selection rules for photo-association transitions.

- Generalised "kets" have been introduced in order to explicitly include the influence of the relative atomic orbital angular momentum of the atoms. In particular all molecular states have been extended by specifying the *total* molecular angular momentum quantum number P and its projection M_P on the space-fixed z-axis.

- These generalised kets allow for exact calculation of collision processes since we can now apply the very fundamental conservation of total angular momentum in the system (= "molecule" + laser field).

- Starting from a simplified model, that yet contains all relevant features of a general continuum ground-state, an expression for the transition probability per unit time from this continuum state to a bound state has been derived. In particular the incoherence and the relative distribution of the relative atomic orbital angular momenta in the ground-state has been determined.

- The angular part of the transition matrix element associated with the photo-association process has been determined exactly and explicitly. This part contains the important selection rules for the transitions.

Summarising the above conclusions:

Using the methods outlined in this report, one can calculate the theoretical photo-association spectra that entail the important selection rules based on general conservation laws. Comparison of these theoretical spectra and experimental high resolution data may be used to extract accurate values for the potential parameters that describe the interaction between two colliding atoms.

Bibliography

[1] J.Prodan, A. Migdall, W.D. Phillips, I. So, H. Metcalf and J. Dalibard,
Phys. Rev. Lett. **54**, 992 (1985)

[2] E.L. Raab, M. Prentiss, A. Cable, S. Chu and D.E. Pritchard,
Phys. Rev. Lett. **59**, 2631 (1987)

[3] R. Thompson,
Nature **362**, 789 (1993)

[4] E. Tiesinga, B.J. Verhaar, H.T.C. Stoof and D. van Bragt,
Phys. Rev. A **45**, 2671 (1992)

[5] A.J. Moerdijk, W.C. Stwalley, R.C. Hulet and B.J. Verhaar,
Phys. Rev. Lett. **72**, 40 (1994)

[6] W. Weikenmeier, U. Diemer, M. Wahl, M. Raab, W. Demtöder and W. Müller,
J. Chem. Phys.**82**, 5354 (1985)

[7] B.J. Verhaar, K. Gibble and S. Chu,
Phys. Rev. A **48**, R3429 (1993)

[8] A.J. Moerdiijk and B.J. Verhaar,
Phys. Rev. Lett. **73**, 518 (1994)

[9] J.D. Miller, R. A. Cline and D.J. Heinzen,
Phys. Rev. A **47**, R4567 (1993)

[10] J.P. Gordon and A. Ashkin,
Phys. Rev. A **21**, 1606 (1980)

[11] J. Dalibard and C. Cohen-Tannoudji,
J. Opt. Soc. Am. B **2**, 1707 (1985)

[12] H.M.J.M. Boesten and B.J. Verhaar,
Phys. Rev. A **49**, 4240 (1994)

[13] S. Kuppens,
graduation report, not published

[14] N.R. Newbury, C.J. Myatt, E.A. Cornell and C.E. Wieman,
Book of abstracts International Conference on Atomic Physics, 1994, 1M-6

[15] C.R. Monroe, E.A. Cornell, C.A. Sackett, C.J. Myatt and C.E. Wieman,
Phys. Rev. Lett. **70**, 414 (1993)

[16] K.B. Davis, M-O. Mewes, M.A. Joffe and W. Ketterle,
Book of abstracts International Conference on Atomic Physics, 1994, 1M-3

[17] P.S. Julienne, A.M. Smith and K. Burnett,
in *Advances in Atomic, Molecular and Optical Physics,*
edited by D.R. Bates and B. Bederson (Academic Press, San Diego, 1992)

[18] C. Amiot,
J. Chem. Phys. **93**, 8591 (1990)

[19] M. Krauss and W.J. Stevens,
J. Chem. Phys. **93**, 4236 (1990)

[20] H.R. Thorsheim, J. Weiner and P.S. Julienne,
Phys. Rev. Lett. **58**, 2440 (1987)

[21] J.D. Miller, R.A. Cline and D.J. Heinzen,
Phys. Rev. Lett. **71**, 2204 (1993)

[22] A.R. Edmonds,
Angular momentum in quantum mechanics,
Princeton University Press (1957)

[23] J. Martens,
Afstudeerverslag THE (1985), not published

[24] M.P.I. Manders,
PhD thesis TUE (1988), not published

[25] M. Born and J.R. Oppenheimer,
Annalen der Physik **84**, 457 (1927)

[26] A. van Heel,
stageverslag TUE (1993), not published

[27] H.T.C. Stoof,
PhD thesis TUE (1989), not published

[28] W. Heitler and F. London,
Z. Phys. **44**, 455 (1927)

[29] F. Spiegelmann, D. Pavolini and J.-P. Daudley,
J. Phys. B. **22**, 2465 (1989)

[30] B. Bussery and M. Aubert-Frécon,
J. Chem. Phys. **82**, 3224 (1985)

[31] F. Maeder and W. Kutzelnigg,
Chem. Phys. **42**, 195 (1979)

[32] M. Marinescu, H.R. Sadeghpour and A. Dalgarno,
Phys. Rev. A. **49**, 982 (1994)

[33] A. Dalgarno and W. D. Davision,
Adv. At. Mol. Phys. **2**, 1 (1966)

[34] M.L. Manakov and V.O. Ovsiannikov,
J. Phys. B. **10**, 569 (1985)

Appendix

In this appendix, we give the derivation that takes us from (6.13) to (6.14). Thus we start with:

$$\kappa := < \tilde{L}|\tilde{\Lambda}|\tilde{S}\tilde{\Sigma}\tilde{P}\tilde{M}_P|\vec{d}\cdot\vec{E}_L|SM_SNM_N;z > \tag{.1}$$

Now we express $|SM_SNM_N;z>$ in the body-fixedstates, using equation (4.15)

$$|SM_SNM_N;z> = \sum_{P,M_P}\sum_{\Omega}(-1)^{S-\Omega} < SM_SNM_N|PM_P > < S-\Omega P\Omega|N0 > |S\Omega PM_P > \tag{.2}$$

and for $|\tilde{L}|\tilde{\Lambda}|\tilde{S}\tilde{\Sigma}\tilde{P}\tilde{M}_P>$ of well-defined total parity we substitute

$$|\tilde{L}|\tilde{\Lambda}|\tilde{S}\tilde{\Sigma}\tilde{P}\tilde{M}_P > = \frac{1}{2}\frac{1}{\sqrt{2(1+\delta_{\tilde{\Lambda}0}\delta_{\tilde{\Sigma}0})}}\sqrt{\frac{2\tilde{P}+1}{8\pi^2}}[|\tilde{L}\tilde{\Lambda}\tilde{S}\tilde{\Sigma}>D^{\tilde{P}*}_{\tilde{M}_P\tilde{\Omega}}(\alpha,\beta,\gamma)+$$
$$+(-1)^{P+L+S}|\tilde{L}\tilde{-\Lambda}\tilde{S}\tilde{-\Sigma}>D^{\tilde{P}*}_{\tilde{M}_P\tilde{-\Omega}}(\alpha,\beta,\gamma)] \tag{.3}$$

Upon these replacements κ transforms into:

$$\kappa = \frac{1}{2}\frac{1}{\sqrt{2(1+\delta_{\tilde{\Lambda}0}\delta_{\tilde{\Sigma}0})}}\sqrt{\frac{2\tilde{P}+1}{8\pi^2}}\int_0^{2\pi}d\alpha\int_0^{\pi}\sin(\beta)d\beta\int_0^{2\pi}d\gamma$$
$$\sum_{n=-1}^{1}\sum_{q=-1}^{1}\sum_{P,M_P}\sum_{\Omega}\sqrt{\frac{2P+1}{8\pi^2}}(-1)^{S-\Omega+q} < SM_SNM_N|PM_P > < S-\Omega P\Omega|N0 >$$
$$\left[< \tilde{L}\tilde{\Lambda}\tilde{S}\tilde{\Sigma}|d'_q|00S\Omega > D^{\tilde{P}}_{\tilde{M}_P\tilde{\Omega}}(\alpha,\beta,\gamma)D^{1}_{n-q}(\alpha,\beta,\gamma)D^{P*}_{M_P\Omega}(\alpha,\beta,\gamma)E_n\right]+$$
$$(-1)^{\tilde{P}+\tilde{L}+\tilde{S}}\left[< \tilde{L}\tilde{-\Lambda}\tilde{S}\tilde{-\Sigma}|d'_q|00S\Omega > D^{\tilde{P}}_{\tilde{M}_P\tilde{-\Omega}}(\alpha,\beta,\gamma)D^{1}_{n-q}(\alpha,\beta,\gamma)D^{P*}_{M_P\Omega}(\alpha,\beta,\gamma)E_n\right] \tag{.4}$$

Since the electron spin is not affected by the electronic transitions, this simplifies to:

$$\kappa = \frac{1}{2}\frac{1}{\sqrt{2(1+\delta_{\tilde{\Lambda}0}\delta_{\tilde{\Sigma}0})}}\sqrt{\frac{2\tilde{P}+1}{8\pi^2}}\int_0^{2\pi}d\alpha\int_0^{\pi}\sin(\beta)d\beta\int_0^{2\pi}d\gamma\sum_{n=-1}^{1}\sum_{q=-1}^{1}$$

$$\sum_{P,M_P}\sum_{\Omega}\delta_{\tilde{S}S}\sqrt{\frac{2P+1}{8\pi^2}}(-1)^{S-\Omega+q} < SM_SNM_N|PM_P > < S-\Omega P\Omega|N0 >$$

$$\left[< \tilde{L}\tilde{\Lambda}|d'_q|00 > \delta_{\tilde{\Sigma}\Omega}D^{\tilde{P}}_{\tilde{M}_P\tilde{\Omega}}(\alpha,\beta,\gamma)D^{1}_{n-q}(\alpha,\beta,\gamma)D^{P^*}_{M_P\Omega}(\alpha,\beta,\gamma)E_n\right] +$$

$$+(-1)^{\tilde{P}+\tilde{L}+S}\left[< \tilde{L}\tilde{-\Lambda}|d'_q|00 > \delta_{-\tilde{\Sigma}\Omega}D^{\tilde{P}}_{\tilde{M}_P-\tilde{\Omega}}(\alpha,\beta,\gamma)D^{1}_{n-q}(\alpha,\beta,\gamma)D^{P^*}_{M_P\Omega}(\alpha,\beta,\gamma)E_n\right] \quad (.5)$$

In order to further simplify this large expression, we use some properties of the Wigner-D-funcions (see for example Edmonds [22]):

$$D^{l*}_{mk}(\alpha,\beta,\gamma) = (-1)^{m-k}D^{l}_{-m-k}(\alpha,\beta,\gamma) \quad (.6)$$

and

$$\int_0^{2\pi}d\alpha\int_0^{\pi}\sin(\beta)d\beta\int_0^{2\pi}d\gamma D^{a}_{m_ak_a}(\alpha,\beta,\gamma)D^{b}_{m_bk_b}(\alpha,\beta,\gamma)D^{c}_{m_ck_c}(\alpha,\beta,\gamma) = \quad (.7)$$

$$8\pi^2\begin{pmatrix} a & b & c \\ m_a & m_b & m_c\end{pmatrix}\begin{pmatrix} a & b & c \\ k_a & k_b & k_c\end{pmatrix}$$

Then the expression for κ simplifies to

$$\kappa = \frac{1}{2}\frac{1}{\sqrt{2(1+\delta_{\tilde{\Lambda}0}\delta_{\tilde{\Sigma}0})}}\sqrt{(2\tilde{P}+1)}\delta_{S\tilde{S}}\sum_{n}\sum_{q}\sum_{P,M_P}\sum_{\Omega}$$

$$\sqrt{2P+1}(-1)^{q} < SM_SNM_N|PM_P > < S-\Omega P\Omega|N0 >$$

$$\left[\delta_{\tilde{\Sigma}\Omega} < 1\tilde{\Lambda}|d'_q|00 > (-1)^{M_P-\Omega}\begin{pmatrix} \tilde{P} & 1 & P \\ \tilde{M}_P & n & -M_P\end{pmatrix}\begin{pmatrix} \tilde{P} & 1 & P \\ \tilde{\Omega} & -q & -\Omega\end{pmatrix}E_n\right] +$$

$$\left[(-1)^{\tilde{P}+\tilde{L}+S}\delta_{-\tilde{\Sigma}\Omega} < 1-\tilde{\Lambda}|d'_q|00 > (-1)^{M_P-\Omega}\begin{pmatrix} \tilde{P} & 1 & P \\ \tilde{M}_P & n & -M_P\end{pmatrix}\begin{pmatrix} \tilde{P} & 1 & P \\ \tilde{-\Omega} & -q & -\Omega\end{pmatrix}E_n\right] \quad (.8)$$

Furthermore, since Ω is an integer and since all excited states have $\tilde{L}=1$ we finally arrive at:

$$\kappa = \frac{1}{2}\frac{1}{\sqrt{2(1+\delta_{\tilde{\Lambda}0}\delta_{\tilde{\Sigma}0})}}\sqrt{(2\tilde{P}+1)}\delta_{S\tilde{S}}\sum_{n}\sum_{q}\sum_{P,M_P}\sum_{\Omega}$$

$$\sqrt{2P+1}(-1)^{q} < SM_SNM_N|PM_P > < S-\Omega P\Omega|N0 >$$

$$\left[\delta_{\tilde{\Sigma}\Omega} < 1\tilde{\Lambda}|d'_q|00 > (-1)^{S+M_P}\begin{pmatrix} \tilde{P} & 1 & P \\ \tilde{M}_P & n & -M_P\end{pmatrix}\begin{pmatrix} \tilde{P} & 1 & P \\ \tilde{\Omega} & -q & -\Omega\end{pmatrix}E_n\right] +$$

$$\left[(-1)^{\tilde{P}+M_P+1}\delta_{-\tilde{\Sigma}\Omega} < 1-\tilde{\Lambda}|d'_q|00 > \begin{pmatrix} \tilde{P} & 1 & P \\ \tilde{M}_P & n & -M_P\end{pmatrix}\begin{pmatrix} \tilde{P} & 1 & P \\ \tilde{-\Omega} & -q & -\Omega\end{pmatrix}E_n\right] \quad (.9)$$